Brain, Behavior, and Immunity 115 (2024) 517–534

Contents lists available at ScienceDirect

Brain Behavior and Immunity

journal homepage: www.elsevier.com/locate/ybrbi

PCSK9 ablation attenuates Aβ pathology, neuroinflammation and cognitive dysfunctions in 5XFAD mice

Antonietta Vilella [a,*], Martina Bodria [a,1], Bianca Papotti [b,1], Ilaria Zanotti [b], Francesca Zimetti [b,*], Giulia Remaggi [b], Lisa Elviri [b], Francesco Potì [c], Nicola Ferri [d,e], Maria Giovanna Lupo [d], Giovanni Panighel [b], Eleonora Daini [a], Eleonora Vandini [b], Michele Zoli [a], Daniela Giuliani [a,1], Franco Bernini [b,1]

[a] Department of Biomedical, Metabolic and Neural Sciences, Center for Neuroscience and Neurotechnology, University of Modena and Reggio Emilia, 41125 Modena, Italy
[b] Department of Food and Drug, University of Parma, 43124 Parma, Italy
[c] Department of Medicine and Surgery, Unit of Neurosciences, University of Parma, 43121, Parma, Italy
[d] Department of Medicine, University of Padova, 35129, Padova, Italy
[e] Veneto Institute of Molecular Medicine (VIMM), 35129, Padova, Italy

ARTICLE INFO

Keywords:
PCSK9
Alzheimer's disease
Microglia
Amyloidosis
Cognitive dysfunction
5XFAD mice

ABSTRACT

Background: Increasing evidence highlights the importance of novel players in Alzheimer's disease (AD) pathophysiology, including alterations of lipid metabolism and neuroinflammation. Indeed, a potential involvement of Proprotein convertase subtilisin/kexin type 9 (PCSK9) in AD has been recently postulated. Here, we first investigated the effects of PCSK9 on neuroinflammation *in vitro*. Then, we examined the impact of a genetic ablation of PCSK9 on cognitive performance in a severe mouse model of AD. Finally, in the same animals we evaluated the effect of PCSK9 loss on Aβ pathology, neuroinflammation, and brain lipids.

Methods: For *in vitro* studies, U373 human astrocytoma cells were treated with Aβ fibrils and human recombinant PCSK9. mRNA expression of the proinflammatory cytokines and inflammasome-related genes were evaluated by q-PCR, while MCP-1 secretion was measured by ELISA. For *in vivo* studies, the cognitive performance of a newly generated mouse line - obtained by crossing 5XFAD^{Het} with PCSK9^{KO} mice – was tested by the Morris water maze test. After sacrifice, immunohistochemical analyses were performed to evaluate Aβ plaque deposition, distribution and composition, BACE1 immunoreactivity, as well as microglia and astrocyte reactivity. Cholesterol and hydroxysterols levels in mouse brains were quantified by fluorometric and LC-MS/MS analyses, respectively. Statistical comparisons were performed according to one- or two-way ANOVA, two-way repeated measure ANOVA or Chi-square test.

Abbreviations: Abs, antibodies; AD, Alzheimer's disease; ANOVA, one-way analysis of variance; APOE, apolipoprotein E; APOER, APOE-interacting receptors; APP, amyloid precursor protein; Aβ, amyloid-β; BACE1, beta-site APP-cleaving enzyme 1; BBB, blood–brain barrier; BHT, butylhydroxytoluene; CA, cornu Ammonis; CC, corpus callosum; Ccl3, chemokine (C-C motif) ligand 3; Ccl6, chemokine (C-C motif) ligand 6; Cd11b, integrin α; -Cg, cingulate cortex; CLA, cell line authentication; CNS, central nervous system; CSF, cerebrospinal fluid; Cst7, cystatin F; Ctx, cerebral cortex; Cx3cr1, CX3C motif chemokine receptor 1; CXP, collision exit potential; CypA, cyclophilin A; D, day; DAB, diaminobenzidine; DG, dentate gyrus; DMEM, Dulbecco's modified Eagle's medium; DP, declustering potential; E, east; EP, entrance potential; FBS, fetal bovine serum; Gapdh, glyceraldehydes-3-phosphate dehydrogenase; GFAP, glial fibrillary acidic protein; HFCD, high fat cholesterol diet; Hip, hippocampus; IBA1, ionized calcium-binding adapter molecule 1; Ifitm3, interferon induced transmembrane protein 3; IHC, immunohistochemistry; IL, interleukin; Ir, immunoreactivity; LC-MS/MS, liquid chromatography-tandem mass spectrometry; LDL, low density lipoprotein LDLR low density lipoprotein receptor; LPL, lipoprotein lipase; LRP1, low-density lipoprotein receptor-related protein 1; MCP-1, monocyte chemoattractant protein-1; Mo, month-old; MWM, Morris water maze; Nctx, neocortex; NLRC4, NLR family CARD domain containing 4; NLRP1, NLR family pyrin domain containing 1; NLRP3, NLR family pyrin domain containing 3; OHC, OH-cholesterol; P2ry12, purinergic receptor P2Y12; PCSK9, proprotein convertase subtilisin/kexin type 9; PS1, presenilin 1; Rer1, retention in endoplasmic reticulum sorting receptor 1; RT, room temperature; S, south; sCtx, somatosensory cortex; SD, standard deviation; SEM, standard error of the mean; SL, stratum lucidum; SO, stratum oriens; SPE, solid phase extraction; SR, stratum radiatum; Stmn1, stathmin 1; SYN, synaptophysin; TC, total cholesterol; ThS, thioflavin-S; TLRs, toll-like receptors; TNFA, tumor necrosis factor α; Wt, wild type.

* Corresponding authors.
E-mail addresses: antonietta.vilella@unimore.it (A. Vilella), francesca.zimetti@unipr.it (F. Zimetti).
[1] These authors equally contributed to the present work.

https://doi.org/10.1016/j.bbi.2023.11.008
Received 27 March 2023; Received in revised form 13 October 2023; Accepted 11 November 2023
Available online 13 November 2023

Results: In vitro, PCSK9 significantly increased *IL6, IL1B* and *TNFA* mRNA levels in Aβ fibrils-treated U373 cells, without influencing inflammasome gene expression, except for an increase in *NLRC4* mRNA levels. *In vivo*, PCSK9 ablation in 5XFAD mice significantly improved the performance at the Morris water maze test; these changes were accompanied by a reduced corticohippocampal Aβ burden without affecting plaque spatial/regional distribution and composition or global BACE1 expression. Furthermore, PCSK9 loss in 5XFAD mice induced decreased microgliosis and astrocyte reactivity in several brain regions. Conversely, knocking out PCSK9 had minimal impact on brain cholesterol and hydroxysterol levels.
Conclusions: In vitro studies showed a pro-inflammatory effect of PCSK9. Consistently, *in vivo* data indicated a protective role of PCSK9 ablation against cognitive impairments, associated with improved Aβ pathology and attenuated neuroinflammation in a severe mouse model of AD. PCSK9 may thus be considered a novel pharmacological target for the treatment of AD.

1. Background

Alzheimer's disease (AD) is a neurodegenerative condition representing the most frequent form of dementia in the elderly. Clinically, it is characterized by a progressive cognitive decline, accompanied by worsening of executive abilities (Therriault et al., 2022). AD causes are still largely unknown, a fact that contributes to the lack of effective interventions to prevent, slow down or reverse the disease progression. Indeed, the available drugs are targeting symptoms, with transient effects, and novel treatments have mostly failed in clinical studies (Burns et al., 2022).

The most investigated pathophysiological processes underlying the disease are the increased extracellular deposition of amyloid-β peptide (Aβ) aggregates and the enhanced intracellular content of hyperphosphorylated tau, forming senile plaques and neurofibrillary tangles, respectively (Edwards, 2019; Jack et al., 2013). However, a growing number of evidence highlights the importance of additional players concurring with the complex AD pathophysiology, including alterations of lipid metabolism (Yin, 2022) and neuroinflammation (Kinney et al., 2018).

The association between lipids and AD is supported by several genetic studies showing that loci and genes involved in cholesterol metabolism are risk factors for AD onset and development (de Rojas et al., 2021; Hollingworth et al., 2011; Jones et al., 2010). The most striking example is the evidence that the gene for ε4 isoform of the apolipoprotein E (*APOE*), the main lipid transporter in the central nervous system (CNS), is one of the most powerful predictive factors for AD onset (Koutsodendris et al., 2022; Liu et al., 2013).

Among brain lipids, cholesterol plays a critical role in the maintenance of neuronal functions (Dietschy and Turley, 2001) and several reports suggest that defects in its homeostasis in CNS are associated with AD (Feringa and van der Kant, 2021; Li et al., 2022).

The Proprotein Convertase Subtilisin/Kexin type 9 (PCSK9), a protein primarily expressed in the liver, plays an important regulatory role in plasma cholesterol levels modulation (Ferri, 2012). Interestingly, PCSK9 is also expressed in the brain, where it may be involved in several relevant processes, including neuronal development and apoptosis (Bingham et al., 2006; Seidah et al., 2003). More recent evidence suggests a potential implication of PCSK9 in the pathogenesis of AD (Adorni et al., 2019). For instance, we and others previously observed increased levels of PCSK9 in the cerebrospinal fluid (CSF) of AD patients compared to control subjects (Courtemanche et al., 2018; Zimetti et al., 2017), with the highest concentrations detected in *APOE* ε4 carriers (Zimetti et al., 2017). Consistently, an increased PCSK9 expression was observed in the frontal cortex of AD patients compared to controls. As well established, this specific brain region is greatly affected by the pathology (Picard et al., 2019).

The mechanisms underlying PCSK9 involvement in AD may relate to the ability to degrade the neuronal APOE-interacting receptors (APOERs), as occurs for the low-density lipoprotein receptors (LDLR) in the liver (Kysenius et al., 2012; Poirier et al., 2008). This activity may interfere with neuronal cholesterol uptake, the sole process warrantying cholesterol supply to adult neurons, for the maintenance of physiological functions (Mahley, 2016). Other possible mechanisms may rely on PCSK9 reported pro-apoptotic effect (Liu et al., 2017; Poirier et al., 2008). In support of these hypotheses, we recently demonstrated that PCSK9 affects astrocytic and neuronal cholesterol metabolism, by degrading ApoER2 and LDLR and leading to neuronal cholesterol depletion. Moreover, PCSK9 worsened the neurotoxic effect induced by Aβ fibrils (Papotti et al., 2022). In addition, others reported that PCSK9, by targeting also the low-density lipoprotein receptor-related protein 1 (LRP1), may reduce the clearance of Aβ peptide through the blood–brain barrier (BBB), thus favouring plaques deposition in the brain (Mazura et al., 2022). Finally, PCSK9 may additionally exert a pro-inflammatory effect on cerebral cells, as previously reported in macrophages (Badimon et al., 2021; Jaen et al., 2022; Ricci et al., 2018; Tang et al., 2017). In this regard, the neuroinflammatory effect of PCSK9 has not been investigated yet.

All the above findings point to PCSK9 as a potential pharmacological target for the treatment of AD. However, despite this set of evidence, the relationship between PCSK9 and AD is still largely unknown and not fully supported by genetic studies, that did not provide convincing indications of the association between PCSK9 variants and disease risk (Bellenguez et al., 2022; Benn et al., 2017; Paquette et al., 2018; Picard et al., 2019).

Thus, in order to shed more light into PCSK9 pathophysiological role in AD, in the present study we first investigated the effects of PCSK9 on neuroinflammation *in vitro*. Then, we evaluated the impact of the genetic ablation of PCSK9 in 5XFAD mice, a severe mouse model of AD, on a number of parameters including cognitive performance, Aβ plaque deposition, distribution and composition, microglia and astrocyte reactivity, neuroinflammatory indexes, and the levels of cholesterol and its main oxidative metabolites in brain and serum.

2. Methods

2.1. In vitro inflammation studies

For *in vitro* inflammation studies, U373-MG human astrocytoma cell line was used. Cells were kindly donated by Prof. Bussolati from the Department of Medicine and Surgery of the University of Parma (Italy). Before use, the cell line underwent authentication by the Cell Line Authentication (CLA) service (Eurofins Genomic, Ebersberg, Germany). Cells were cultured in Dulbecco's Modified Eagle's Medium (DMEM) High Glucose supplemented by 10 % Fetal Bovine Serum (FBS), 1 % penicillin/streptomycin solution (10.000 U/mL and 10 mg/mL, respectively), 1 % L-glutamine 200 mM and 1 % non-essential amino acids 100X solution. Cell culture reagents were from EuroClone (Milan, Italy). Aβ was purchased from Bachem (cat. n. 4014447.1000) and recombinant human PCSK9 was purchased from Cayman Laboratories (cat. n. 20631).

To evaluate the influence of PCSK9 on inflammation, cells were treated for 24 h (h) with human recombinant PCSK9 (5 μg/ml), then incubated for the following 24 h with Aβ fibrils (1 μM), prepared from

monomers as previously described (Papotti et al., 2022). At the end of the incubation, total mRNA was extracted by means of iScriptTM RNA extraction kit Bio-Rad and 1 μl of total extract was used for the one-step qPCR reaction (one-step qPCR SYBR mix, A&A Biotechnology) using specific primer mix combinations (Table 1). *18S* was used as loading control in each experiment.

For the evaluation of monocyte chemoattractant protein-1 (MCP-1) secretion, after treatment of cells as described above, medium was collected and ELISA assay was performed, using the human MCP-1 ELISA kit (R&D System, cat. n. DCP00; Intra- and inter-assay variability is 5 %). Data are shown as mean ± standard deviation (SD) and statistical comparisons were performed using the one-way ANOVA followed by the Tukey's multiple comparison test. A value of $p < 0.05$ was considered statistically significant.

2.2. Animals

A transgenic mouse line was generated by multiple crossings between 5XFAD+/- (5XFAD^{Het}) mice and PCSK9-/- (PCSK9^{KO}) mice. The 5XFAD transgenic mouse model of AD co-overexpresses a triple-mutant human amyloid precursor protein (APP) (Swedish mutation: K670N, M671L; Florida mutation: I716V; London mutation: V717I) and a double-mutant human presenilin 1 (PS1) (M146L and L286V mutations) under the transcriptional control of the neuron-specific Thy-1 promoter. Progenitors with no retinal degeneration allele Pde6brd1 were purchased from Jackson Laboratories (Bar Harbor, ME, USA) and first-

Table 1
List of primers used for Real-Time PCR analyses.

Function	Transcript	NCBI Ref Seq	Primer	sequence (5′- 3′)
Housekeeping genes	*Gapdh*	NM_008084.3	Fw	CAAGGTCATCCATGACAACTTTG
			Rv	GGGCCATCCACAGTCTTCTG
	CypA	NM_008907.2	Fw	AGCATACAGGTCCTGGCATC
			Rv	TTCACCTTCCCAAAGACCAC
	Rer1	NM_026395.2	Fw	CCACCTAAACCTTTTCATTGCG
			Rv	TTTGTAGCTGCGTGCCAAAAT
Lipid-related genes	*Apoe*	NM_001305843.1	Fw	TGTGGGCCGTGCTGTTGGTC
			Rv	GCCTGCTCCCAGGGTTGGTTG
	Lpl	NM_008509.2	Fw	GGATGGACGGTAACGGGAAT
			Rv	GGCCACATCATTTCCCACCA
	Lrp1	NM_008512.2	Fw	AAGGATGACTGTGGAGAC
			Rv	ACTACAGCCACCATTATTC
	Lrp5	NM_008513.3	Fw	CAGTGTGCCCCTCTATGACC
			Rv	CGAATGACGTAGGGCCTGTA
	Cd36	NM_001159558.1	Fw	GGAGCAACTGGTGGATGGTT
			Rv	TACGTGGCCCGGTTCTACTAA
Microglial factors	*Stmn1*	NM_019641.4	Fw	AGGTGCTCCAGAAAGCCATC
			Rv	TCCACGTGCTTGTCCTTCTC
	P2ry12	NM_001357010.1	Fw	CATTGCTGTACACCGTCCTG
			Rv	AACTTGGCACACCAAGGTTC
	Ifitm3	NM_025378.2	Fw	CCGTGAAGTCTAGGGATCGGA
			Rv	GTGTGAAGGTTTTGAGCGTT
	Cd11B	NM_001082960.1	Fw	TACCGTCTACTACCCATCTGGC
			Rv	TTGGTGAGCGGGTTCTGG
	Cx3cr1	NM_009987.4	Fw	ACGGAGACAGTGGCGTTCAG
			Rv	CGGCCAGGCACTTCCTATAC
	Cst7	NM_009977.3	Fw	CAGGAAGACCATGCATCACCA
			Rv	ATAGAGTCCGCTTCAAGGCAG
Inflammatory mediators	*Il1B*	NM_008361.4	Fw	ATCTTTGAAGAAGAGCCCATCC
			Rv	TGTAGTGCAGTTGTCTAATGGG
	Il6	NM_031168.2	Fw	CCTCTCTGCAAGAGACTTCCATCCA
			Rv	GGCCGTGGTTGTCACCAGCA
	TnfA	NM_013693.3	Fw	TCTTCTGTCTACTGAACTTCGG
			Rv	AAGATGATCTGAGTGTGAGGG
	Ccl3	NM_011337.2	Fw	CATATGGAGCTGACACCCCG
			Rv	TCTTCCGGCTGTAGGAGAAGC
	Ccl6	NM_009139.3	Fw	CTGGCCTCATACAAGAAATGGA
			Rv	TTGGAGGGTTATAGCGACGAT
Human primers for *in vitro* analysis				
Housekeeping gene	*18S*	X03205.1	Fw	CGGCTACCACATCCACGGAA
			Rv	CCTGAATTGTTATTTTTCGTCACTACC
Immune cell factors	*Pyrin*	NM_000243	Fw	GTACTTCTCAGAAACCCTGCG
			Rv	AGATGAGGTTGGGGTAAGCG
	NLRP1	NM_033004	Fw	TTCTACGTTGGCCACTTGGG
			Rv	GTGAAGGTACGGCTATGCGG
	NLRP3	NM_001243133	Fw	AAGTGGGGTTCAGATAATGCACG
			Rv	CACTGGAATCTGCTTCTCACG
	NLRC4	NM_001199138	Fw	CCTACAGAATCAACGGCTGC
			Rv	TCAGGCCTTCAGCTAGTTTTATAGC
Inflammatory mediators	*TNFA*	NM_000594	Fw	ACTTTGGAGTGATCGGCC
			Rv	GCTTGAGGGTTTGCTACAAC
	IL6	NM_000600	Fw	GGTACATCCTCGACGGCATCT
			Rv	GTGCCTCTTTGCTGCTTTCAC
	IL1B	NM_000576	Fw	ATGCACCTGTACGATCACTG
			Rv	ACAAAGGACATGGAGAACACC

For each transcript analyzed in *ex-vivo* or *in vitro* experiments, forward (Fw) and reverse (Rv) primer sequences are indicated alongside with general functional classification and NCBI reference.

generation progenies were obtained by crossing 5XFAD^{Het} mice with PCSK9^{KO} breeders. 5XFAD^{Het}PCSK9^{Het} mice were selected and crossed with PCSK9^{KO} mice to obtain 5XFAD^{Het}PCSK9^{KO} mice and related controls (Wt-PCSK9^{Het} and Wt-PCSK9^{KO}, hereinafter mentioned as Ctrls). Mice were kept in conditioned rooms with stable temperature (21 °C) and humidity (60 %), on a light/dark cycle of 12 h; food and water were available *ad libitum*. All animal procedures were approved by the Committee on Animal Health and Care of the University of Modena and Reggio Emilia (protocol number: n° 511/2019-PR) and conducted in accordance with National Institutes of Health guidelines.

2.3. Morris water maze test

Ten month-old (mo) male and female mice were subjected to Morris water maze (MWM) procedure to assess learning and memory as previously described (Runfola et al., 2021). Briefly, mice were placed in a circular white pool with a diameter of 120 cm filled with water at 2 ± 1 °C (made opaque by adding white non-toxic paint), and allowed to swim for 90 seconds (s) or until they found the location of a hidden circular platform with 11 cm diameter; during this learning phase mice were trained with 4 trials per day (starting from a different quadrant with different visual cues at each trial) for 7 days with 30 minutes (min) inter-trial interval and the platform was located in the South (S) quadrant of the pool. For each trial, the time to reach the platform and number of entries into the platform area were analyzed (learning curve Day1-Day7, D1-D7). On the 8th day the platform was moved to East (E) quadrant and two cues were removed; mice underwent a second learning phase consisting in 4 trials per day with a 60 min inter-trial interval between days D8-D13. To assess memory retention, the platform was removed on D14 and the animals were allowed to swim for 60 sec (probe test), and the latency to reach the platform area, total entries in the platform area and the % of time spent in target quadrant were evaluated. The analysis of target search strategy was carried out according to current literature (Vorhees and Williams, 2006). Briefly, spatial accurate strategy and non-spatial strategy were distinguished considering individual swim paths during probe test.

Behavioural test was performed by an operator unaware of the treatment to avoid bias. Animal behaviour was conducted in a sound-proof room, recorded and automatically analyzed with ANY-maze Video Tracking system (Stoelting). Target search strategy was manually scored, independently, by two operators unaware of the treatment.

All data are shown as mean ± standard error of the mean (SEM) and were analysed by one-way ANOVA, two-way repeated measure ANOVA, or chi-square test as appropriate using the statistical package SPSS (version 26). Due to the unequal distribution of male and female mice in the experimental groups, and the documented impact of sex on behaviour and other AD related parameters (Forner et al., 2021; Oblak et al., 2021), the possible effect of sex on experimental parameters was preliminarily tested and when a statistically significant difference was observed, sex was used as a covariate in the subsequent statistical analysis. $p \leq 0.05$ was considered as the level for a significant difference and $0.10 > p > 0.05$ as trend for a significant difference (see Supplementary Table 1 for detailed statistical reports).

2.4. Immunohistochemical analysis

Mice were anaesthetized with isoflurane and sacrificed by intracardiac perfusion with cold 4 % paraformaldehyde and fixed brains were cut at the cryostat (20 μm) and processed according to established protocols to test cell-specific AD alterations by using specific antibodies (Abs) against amyloid plaques and microglial cells through immunohistochemical (IHC) analysis (Daini et al., 2021; Rigillo et al., 2018).

The following Abs were used to test specific AD-linked alterations at synaptic and cellular levels: mouse anti-human Aβ/APP 6E10 (epitope human Aβ1-16, 1:500, Signet, cat. n. 9300–10), mouse anti-human Aβ 11A1 (epitope synthetic peptide of E22P-Aβ 10–35 part, 1:500, Tecan, cat. n. 10379), rabbit anti-ionized calcium-binding adapter molecule 1 (IBA1, 1:1000, Wako, cat. n. 019–19741), rabbit anti-glial fibrillary acidic protein (GFAP, 1:2000, Dako, cat. n. Z0334) and mouse anti-synaptophysin (SYN, 1:1000, SYSY, cat. n. 101111), rabbit anti-beta-site APP-cleaving enzyme 1 (BACE1, 1:1000, Cell Signaling, cat. n. 5606). A pre-treatment with formic acid was performed for anti-Aβ Abs. Vectastain ABC-HRP (cat. n. PK-4002; cat. n. PK-4001) kit was used for peroxidase diaminobenzidine (DAB) stainings; slices were placed on gelatinized glass slides, dehydrated and mounted with Eukitt® mounting medium. Thioflavin-S (ThS, Sigma, cat. n. 1892) and Congo Red (Sigma, cat. n. 6277) stainings were performed according to established protocols (Daini et al., 2021).

2.5. Image and statistical analyses

Immunolabelled brain slices were visualized and photographed on a Nikon Eclipse CiL microscope (10x and 40x objective) through a Nikon DS-Fi3 camera under constant light conditions. Shading error correction was performed before image acquisition to correct for irregularities in the illumination of the microscopic field. All evaluations were performed on coded slides by at least two experimenters.

ThS- or Aβ-immunoreactive plaque analysis was performed on images obtained with a 10x objective. Plaques were manually selected within the neocortex (Nctx) and the hippocampus (Hip) (Bregma between −1.46 and −1.58 mm from (Paxinos and Franklin, 2019)) and morphometric parameters such as plaque number as well as single plaque areas were measured through a Nikon NIS-Elements D software or ImageJ Fiji software.

For SYN and BACE1 immunoreactivity (ir) analysis, three somatosensory cortex (sCtx) (exclusively for SYN) and cornu Ammonis 3 (CA3) fields of Hip slices/mouse (Bregma between −1.46 and −1.58 mm from Paxinos and Franklin, 2019) were acquired with 10x objective before counterstaining with Nissl stain to better delineate the hippocampal subregion boundaries. The semi-quantitative densitometric and morphometric analyses (area, length and thickness) were performed following established protocols (Zoli et al., 1990a; Zoli et al., 1992) using routines from the Nikon NIS-Elements D (5.21.00v) and ImageJ Fiji software. First, images were manually edited to remove edge artefacts, folds, and blood vessels, then thresholded as described (Zoli et al., 1990b).

For densitometric analysis, acquired images were converted to 32-bit grayscale and specific optical density values were obtained by subtracting the optical density of the sampled region from the optical density of non-specific staining, i.e., pyramidal layer for CA3 analysis.

For GFAP and IBA1 analysis, at least three slices/mouse from corpus callosum-cingulate cortex (CC-Cg) (Bregma between −0.5 and −0.9) and Hip (Bregma between −1.46 and −1.58 mm from Paxinos and Franklin, 2019) were acquired with 10x objective. Acquired images were converted to 32-bit grayscale and the following thresholding procedure was applied: for GFAP staining −35, −20, −40, −5 grayscale units from the peak mean gray value for hippocampal CA1 field, CA3 field, dentate gyrus (DG) hilus and CC-Cg; for IBA1 staining −10 grayscale units for CC-Cg and DG hilus; then, % positive area, i.e., the area covered by pixels with a gray value above the threshold, was automatically recorded by means of *analyse particles* function of ImageJ software. As specifically concerns microglial analysis, IBA1 + cell count was performed manually, within the area of interest by using a 10x objective.

Values are shown as mean ± SEM or 95 % confidence interval as appropriate. Group differences between different brain regions were analysed by means of two-way repeated measure ANOVA or two-way ANOVA. When a main effect of genotype was demonstrated, the main effect of PCSK9 expression in AD mice was tested by means of one- or two-way ANOVA as appropriate. Proportions were analysed by means of the chi-square test. Statistical analyses were performed through SPSS software, with $p < 0.05$ as the level for a significant difference and $0.10 > p > 0.05$ as a trend for a significant difference. Detailed statistical

reports are shown in Supplementary Table 1.

2.6. Total cholesterol (TC) quantification in mouse brain and serum

After the sacrifice, the right cerebral hemisphere of mice was weighted and mechanically homogenated. Homogenates underwent lipid extraction with the Folch's Solution (Chloroform: Methanol [2:1] v/v) for 24 h. The lipophilic phase was then evaporated under a nitrogen stream and re-suspended in Reaction Buffer (0.5 M potassium phosphate, 0.25 M NaCl, 25 mM cholic acid and 0.5 % Triton X-100). The fluorometric Amplex® Red Cholesterol assay (Thermo-Fisher Scientific, MA, USA) was used to quantify cholesterol content in lipids extracted from the brain following the manufacturer's instructions. To quantify TC levels in serum, peripheral blood was collected after sacrifice in BD VACUTAINER CAT tube and after 1 h incubation at room temperature (RT), serum was isolated by centrifugation at 2500 rpm for 10 min; then the fluorometric Amplex® Red Cholesterol assay (Thermo Fisher Scientific, MA, USA) was used to quantify TC following the manufacturer's instructions. All data are shown as mean ± SEM. Statistical comparisons between the four genotypes were performed using the two-way ANOVA considering $p \leq 0.05$ as statistically significant and $0.10 > p > 0.05$ as a trend for a significant difference. Statistical comparisons between wild-type (Wt) B6SJL and 5XFAD mice were performed by one-way ANOVA, considering $p < 0.05$ as statistically significant.

2.7. Hydroxysterols quantification in mouse brain and serum

The three main hydroxysterols (24-OH-cholesterol, 25-OH-cholesterol and 27-OH-cholesterol, 24-OHC, 25-OHC and 27-OHC, respectively) quantification in mouse brain and sera was performed by liquid chromatography-tandem mass spectrometry (LC-MS/MS) (Borah et al., 2020; Del Puppo et al., 1998). Specifically, the lipophilic phase extracted through the Folch's solution from the left cerebral hemisphere, as well as from 0.2 ml of serum, were supplemented with Butylhydroxytoluene (BHT, 0.1 μg/μl) and underwent alkaline hydrolysis in 1 ml of 1 M NaOH in 90 % Ethanol for 2 h at 60 °C. One ml of saline was then added and sterols were extracted with 2 ml of Petroleum Ether 40°- 60°. Dried lipid extracts were then resuspended in 2 ml of deionized H_2O supplemented with 5 % v/v of Methanol and oxysterols were separated by Solid Phase Extraction (SPE) Cartridges C18 (Waters, MA, USA), as previously described.

LC-MS/MS analysis was then carried out by adding to each dried sample 100 μl of Methanol enriched with 1 μg/μl of 24-, 25- and 27-deuterated OHC (Avanti Polar Lipids, AL, USA), used as internal standards. Samples were subsequently eluted through a C18 Synergi Hydro-RP column (150 mm x 3 mm, 80A, 4 μm particles; Phenomenex, CA, USA), equipped with a C18 pre-filtering column. The mobile phase was made of Methanol: acetonitrile: H_2O [14:1:0.6], added with 0.1 % v/v formic acid. The elution was isocratic at a flow rate of 200 μl/min for 50 min, the injection volume was 20 μl and each sample was injected in duplicate. The analysis was carried out using an Agilent HP 1200 chromatographic system (Agilent Technologies, CA, USA), with a 100-vial capacity sample tray and coupled with a QTRAP 4000 triple quadrupole mass spectrophotometer (ABSCIEX, CA, USA), equipped with a pneumatically assisted ESI interface. Nitrogen (99.99 % of purity) was used as a sheath gas and the auxiliary gas was delivered at flow rates of 45 and 5 arbitrary units, respectively. Optimized conditions of the interface were set as follows: ESI voltage 5.5 kV; declustering potential (DP) 35 V; entrance potential (EP) 10 V; collision exit potential (CXP) 10 V and capillary temperature 350 °C. Experiments were performed under positive ion-selected reaction monitoring conditions, using nitrogen as a collision gas (pressure of 2.1 x 10^{-3} mbar). The analytical method performed was initially set up by using 24-, 25- and 27-OHC spiked with 1 μg/μl of the respective deuterated internal standard. All data are shown as mean ± SEM and statistical comparisons were performed with one or two-way ANOVA as appropriate.

2.8. Total RNA extraction, reverse transcription, and real-time polymerase chain reaction (ex vivo)

A separate group of mice was sacrificed under deep anaesthesia through intracardiac injection of cold PBS, the brain was dissected out and cerebral cortex (Ctx) was lysed by mechanical disruption in Trizol reagent (Qiagen), homogenized following the procedure provided by the manufacturer (RNeasy Plus Mini Kit, Qiagen) and processed for qPCR as described (Villacampa et al., 2015). Isolated mRNA was reverse transcribed to cDNA using random hexamers and M−MLV Reverse Transcriptase (Promega Corporation) following the instructions provided by the manufacturer. Samples were heated at 70 °C for 5 min to eliminate any secondary structures, then incubated at 23 °C for 10 min, 1 h at 37 °C, and 5 min at 95 °C before being chilled at 4 °C using a thermocycler T Gradient (SimpliAmp, Applied Biosystem). The amount of cDNA was quantified with iTaq Universal SYBR Green Supermix (Bio-Rad) using a Bio-Rad RT-PCR iCycler. Each PCR reaction was performed in triplicate using 300 nM of each primer (Table 1), 10 μl of iTaq Universal SYBR Green Supermix (Bio-Rad), cDNA and nuclease-free water with the following cycling parameters: 2 min at 95 °C and 40 cycles of 5 min at 95 °C and 30 sec at 60 °C, followed by 5 sec at 95 °C and 65° to 95 °C melting curve analysis.

2.9. PCR product and statistical analyses (ex vivo)

For gene expression analysis, mRNA levels of each experimental gene target were normalized to the average of three housekeeping genes. Glyceraldehydes-3-phosphate dehydrogenase (*Gapdh*), retention in endoplasmic reticulum sorting receptor 1 (*Rer1*) and cyclophilin A (*CypA*) reference genes were used as endogenous controls. For quantitative evaluation of changes, the comparative ΔΔCt method was performed, using as a calibrator the average levels of expression of Wt-$PCSK9^{Het}$ or B6SJL mice. Statistical comparisons were performed using one- or two-way ANOVA as appropriate, considering a value of $p \leq 0.05$ as statistically significant and $0.10 > p > 0.05$ as a trend for a significant difference.

2.10. Protein extraction and western blotting analysis (ex vivo)

Dissected Hip was homogenized by mechanical disruption in Lysis Buffer (100 mM Tris/HCL, pH 7.5, 150 mM NaCl, 1.0 mM EDTA, 1 % deoxycholate sodium, 1 % TritonX100, 0.01 % SDS, protease and phosphatase inhibitor cocktails). Total proteins were extracted and quantified by using standard Pierce bicinconic acid assay (BCA) as previously described (Almolda et al., 2015). After quantification, proteins (5 μg for each sample) were denatured, electrophoretically separated, and transferred onto PVDF membranes. The blots were then blocked and incubated overnight at 4 °C with blocking buffer containing the primary Ab: mouse anti-synaptophysin (SYN, 1:1000, SYSY, cat. n. 101111) and rabbit anti- βtubulin (Tub, 1:2000, Cell Sign, cat. n. 2146S). The following day, the membranes were incubated with a specific secondary anti-rabbit or mouse IgG-HRP-linked Ab for 1 h at room temperature. The membranes were analysed by the enhanced chemiluminescence system according to the manufacturer's protocol (Pierce). The protein signals were quantified by means of GelPro analyzer and expressed as relative optical density (OD) normalized over Tub.

All data are shown as mean ± SEM. Values were analyzed by two-way ANOVA using SPSS; sex was used as covariate. Differences were considered significant with p value < 0.05.

3. Results

3.1. Effects of PCSK9 on Aβ-induced inflammation in vitro

To define the potential involvement of PCSK9 in Aβ-induced inflammatory response, we performed *in vitro* studies using the U373

astrocytoma cell line (Giovannoni and Quintana, 2020). We first defined the inflammatory response of U373 to Aβ fibrils, in order to simulate an AD-like condition (Papotti et al., 2022). As shown in Fig. 1, Aβ fibrils (1 μM) slightly upregulated the mRNA expression of interleukin 6 (*IL6*) and interleukin 1 beta (*IL1B*), without inducing significant changes in tumour necrosis factor-alpha (*TNFA*). Importantly, recombinant PCSK9 (5 μg/ml) stimulated *IL6* expression, and the co-incubation of both Aβ fibrils and recombinant PCSK9 further induced the levels of all these cytokines, suggesting a strengthening proinflammatory action of PCSK9 on basal Aβ fibrils activity. As reported previously, the Aβ-induced release of proinflammatory cytokines by astrocytes depends on the expression of several receptors implicated in cell activation, such as the CD36 receptor. In addition, the binding of Aβ to the CD36 receptor triggers the assembly of a heterotrimeric complex with the Toll-like receptors (TLRs) 4 and 6, an essential step for host defence against pathogens (Giovannoni and Quintana, 2020). Based on these premises, we evaluated the impact of PCSK9 on these receptors, but we found that PCSK9 was not able to modulate *CD36, TLR-4* or *TLR-6* gene expression (not shown).

To extend the data of proinflammatory cytokines gene expression, we performed an additional analysis by measuring the release of MCP-1 into the media by ELISA. This analysis revealed that Aβ fibrils significantly increased the release of this chemokine from U373 cell line, and this effect was further enhanced by the co-incubation with PCSK9 (Fig. 2).

The effect of Aβ and PCSK9 on cytokine mRNA levels prompted us to investigate the expression of inflammasome genes, such as *Pyrin*, Nucleotide-binding oligomerization domain, Leucine-rich Repeat and Pyrin domain containing 1 and 3 (*NLRP1* and *NLRP3*), NLR family caspase recruitment domain (CARD)–containing protein 4 (*NLRC4*), the complex that induces the activation and release of IL1β (Man and Kanneganti, 2015). As expected, Aβ significantly upregulated *NLRP1*, *NLRC4* and *NLRP3* and the co-incubation with PCSK9 had a strenghtening effect on mRNA levels of *Pyrin* and *NLRC4*, despite it was statistically significant only for *NLRC4* (Fig. 3). These data further support the contribution of PCSK9 on inflammatory response in U373 astrocytoma cell line already exposed to Aβ fibrils.

3.2. Effects of PCSK9 loss in 5XFAD mice

3.2.1. Spatial learning and memory

In order to assess whether the absence of PCSK9 influenced the cognitive impairment in our *in vivo* model, spatial learning and memory were tested.

The performance of B6SJL and 5XFAD mice was preliminarily compared in the MWM test, confirming a significant decrease in spatial learning abilities and memory in 10 mo 5XFAD mice (**Supplementary Fig. 1A,B**). Subsequently, the MWM test was performed comparing Wt-PCSK9^{Het}, Wt-PCSK9^{KO}, 5XFAD-PCSK9^{Het} and 5XFAD-PCSK9^{KO} mice. Swim speed of all tested groups did not differ throughout the experiment (not shown). Repeated measure two-way ANOVA analysis demonstrated that the learning curves of the groups were significantly different with a main effect of the 5XFAD factor (Fig. 4**A**). In addition, the analysis in 5XFAD mice showed that the escape latency to reach the hidden platform was significantly reduced by PCSK9 loss, reaching values not statistically different from those of Ctrls mice (Fig. 4 **A** and Supplementary Table 1). Twenty-four hours after the last training session, mice underwent a 60 sec probe test, measuring the % time spent in the target quadrant (E quadrant). The analysis demonstrated a significant main effect of the 5XFAD factor, but no significant difference between the two 5XFAD mouse groups (Fig. 4 **B**). Occupancy plots for grouped data showing the development of a quadrant- and platform position-specific preference are reported in Fig. 4 **C**.

To assess the qualitative aspects of learning in the MWM task we analyzed the search strategies displayed by the mice as a measure of the accuracy of swim trajectories used to find the platform location during the probe session. The search strategy analysis demonstrated that 5XFAD-PCSK9^{KO} mice have a statistically significant increase in spatially directed strategies and a decrease in non-targeted search strategies (random and non-cognitive) with respect to 5XFAD-PCSK9^{Het} mice (Fig. 4 **C-D**).

Altogether, these results indicate that PCSK9 loss in 5XFAD mice is associated with an improvement in learning and memory performance accompanied by an ameliorated search strategy to locate platform position. The detailed statistical report is summarized in Supplementary Table 1.

3.2.2. Amyloid plaques

It is known that Aβ deposition, a key neuropathological factor in AD development, is a precocious event in 5XFAD mice (Daini et al., 2021). In order to investigate whether improved behavioral performance was associated with a reduction in AD-like neuropathology, brain slices from 10 mo Ctrls, 5XFAD-PCSK9^{Het} and 5XFAD-PCSK9^{KO} mice were processed for IHC plaque visualization. Antibodies for Aβ and APP (anti-6E10 Ab) or Aβ42 neurotoxic oligomers (anti-11A1 Ab), as well as ThS standard staining for β-sheet structures and thus a marker for fibrillar

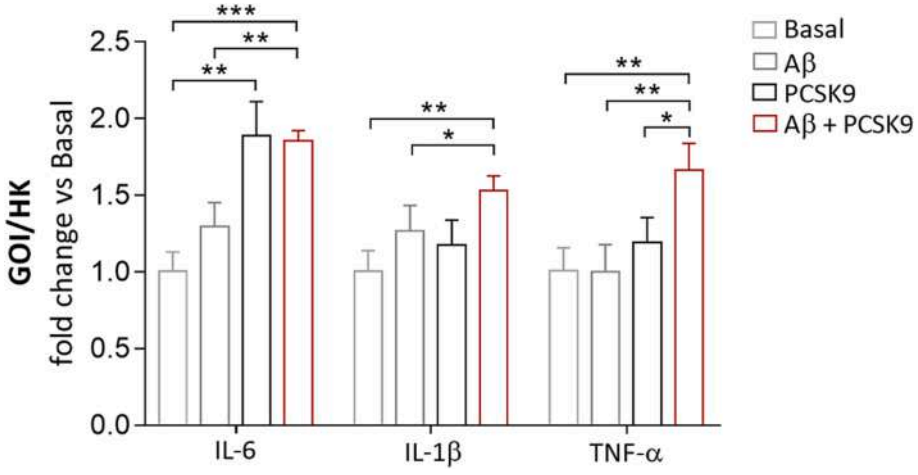

Fig. 1. Effect of Aβ fibrils and PCSK9 on cytokines mRNA expression in U373 astrocytoma cell line. U373 cells were treated for 24 h with human recombinant PCSK9 (5 μg/ml), then incubated for the following 24 h with Aβ fibrils (1 μM). At the end of the incubation total RNA was extracted and real-time qPCR was performed. Experimental conditions were tested in triplicate and data are expressed as mean ± SD. Statistical analyses were performed using the one-way ANOVA with a Tukey's multiple comparison test (Supplementary Table 1); * $p < 0.05$; ** $p < 0.01$; *** $p < 0.001$.

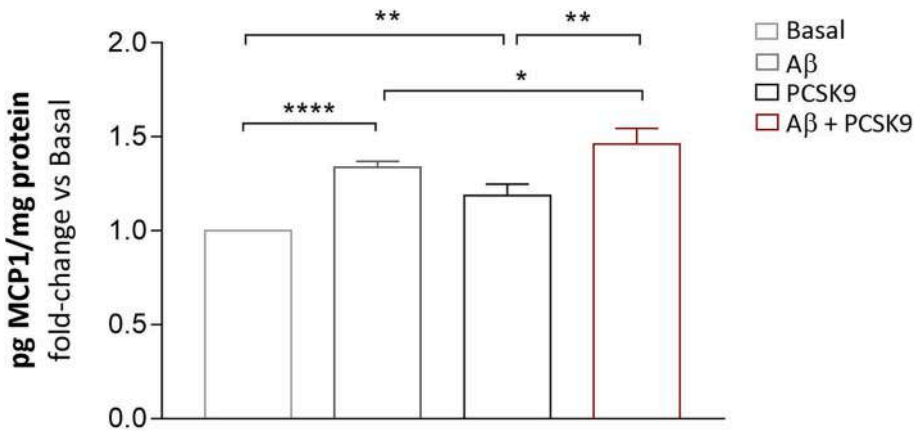

Fig. 2. Effect of Aβ fibrils and PCSK9 on MCP-1 secretion from U373 astrocytoma cell line. U373 cells were treated for 24 h with human recombinant PCSK9 (5 μg/ml), then incubated for the following 24 h with Aβ (1 μM). At the end of the incubation the conditioned media were collected, and ELISA was performed. Experimental conditions were tested in triplicate and data are expressed as mean ± SD fold change vs basal. Statistical analyses were performed using the one-way ANOVA with a Tukey's multiple comparison test (Supplementary Table 1); * $p < 0.05$; ** $p < 0.01$; **** $p < 0.0001$.

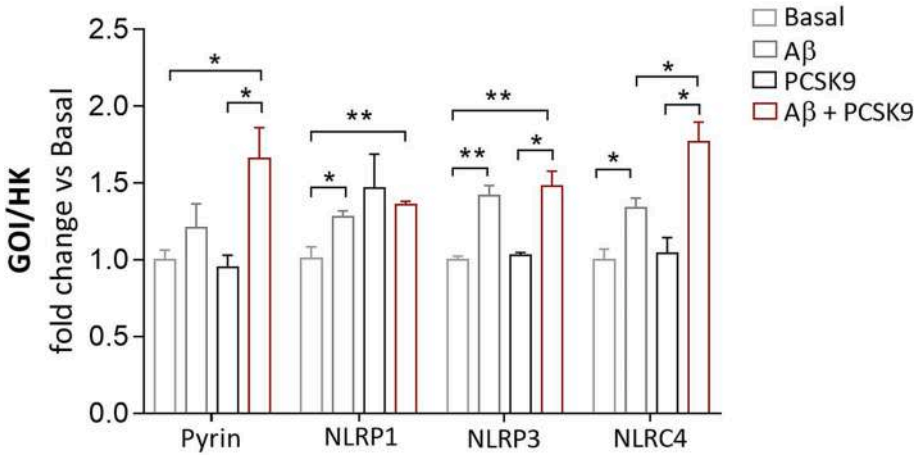

Fig. 3. Effect of Aβ fibrils and PCSK9 on inflammasome mRNA expression in U373 astrocytoma cell line. U373 cells were treated for 24 h with human recombinant PCSK9 (5 μg/ml), then incubated for the following 24 h with Aβ fibrils (1 μM). At the end of the incubation the conditioned media were collected, and real-time qPCR was performed. Experimental conditions were tested in triplicate and data are expressed as mean ± SD. Statistical analyses were performed using the one-way ANOVA with a Tukey's multiple comparison test (Supplementary Table 1); * $p < 0.05$; ** $p < 0.01$.

and compact Aβ, were used. After staining, the number of protein aggregates as well as the mean % area occupied by Aβ ir or ThS stain were compared.

Fig. 5 provides representative images of hippocampal (DG, Fig. 5 **A-B**) and cortical (Nctx, Fig. 5 **E-F**) ThS^+ amyloid plaques and their relative quantification (Fig. 5 **C,D,G,H**). Our analysis demonstrated the selective presence of ThS^+ β-sheet-rich protein aggregates in both 5XFAD-$PCSK9^{KO}$ and 5XFAD-$PCSK9^{Het}$ (Fig. 5 **A-B, E-F**) but never in Ctrls (not shown). A significant reduction (-40 %) in the number of ThS^+ amyloid plaques was observed in both DG and Nctx of 5XFAD-$PCSK9^{KO}$ mice with respect to 5XFAD-$PCSK9^{Het}$ mice (Fig. 5 **C,G** respectively). In the same brain areas, the reduction in ThS^+ plaque number was paralleled by a similar reduction in ThS^+ plaque area (Fig. 5 **D,H**). All statistical data are summarized in Supplementary Table 1.

We further characterized amyloid plaques by means of IHC analyses with mouse anti-human Aβ/APP 6E10 Ab (Fig. 6 **A, E, C, G**) and mouse anti-human Aβ 11A1 Ab (Fig. 6 **B, F, D,H**). According to previous results, a significant reduction in the number of $6E10^+$ and $11A1^+$amyloid plaques was observed in both DG (-35 % and −28 %, respectively) and Nctx (-40 % and −36 %, respectively) of 5XFAD-$PCSK9^{KO}$ mice with respect to 5XFAD-$PCSK9^{Het}$ mice. In addition, a specific decrease in the area of $6E10^+$ plaques was observed in both analyzed brain areas while $11A1^+$ areas were unaffected (Fig. 6 **I-L** and Supplementary Table 1 for statistical report). Since we observed that the amyloidosis process was more pronounced in the Nctx than in the Hip of 10 mo 5XFAD mice (Figs. 5-6), we first evaluated if the ratio between hippocampal and cortical plaque load was influenced by genotypes.

We observed that in 5XFAD-$PCSK9^{Het}$ mice the number and area of ThS^+ and of $11A1^+$ plaques were similar, and smaller than those of $6E10^+$ plaques. In 5XFAD-$PCSK9^{KO}$ mice, despite a global and significant decrease of amyloidosis was observed, the ratio between differently stained plaques was maintained (Fig. 6 **I-L** and Supplementary Table 1 for statistical report). Finally, our results did not evidence any significant genotype-related change in the DG/Nctx ratio of the number of Aβ-stained plaques, that was about 10 % for both ThS^+ and $11A1^+$ and 15 % for $6E10^+$ plaques, suggesting that the spatial/regional distribution of Aβ plaques was maintained in the absence of PCSK9 (Fig. 6 **M** and Supplementary Table 1 for statistical report).

We then performed an analysis of the size distribution of amyloid plaques. Amyloid plaques in the hippocampal DG and Nctx of 5XFAD mice were stratified according to their size into four ranges. In accordance with reduced amyloidosis (see above), the number of $A\beta^+$ plaques for each size range were reduced in 5XFAD-$PCSK9^{KO}$ mice (not shown). On the other hand, the proportion of plaques in the different size ranges

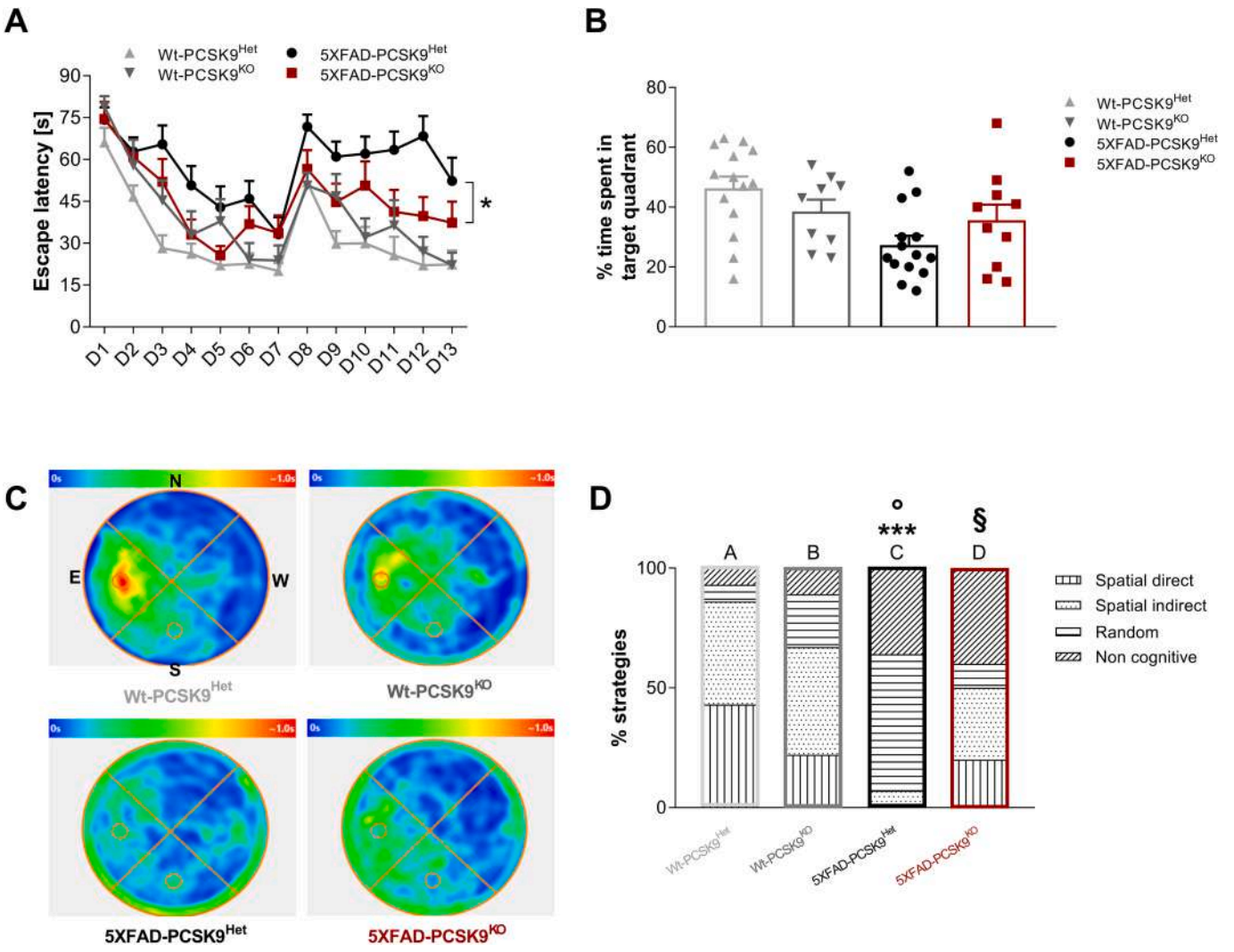

Fig. 4. The loss of PCSK9 improves both learning and memory in AD mice. A Analysis of MWM learning curve. The time needed to find the platform (escape latency) was averaged for each day (4 trials/day) and analyzed by a two-way repeated measures ANOVA with training day and genotype as factors and sex as covariate. The comparison between 5XFAD groups was performed by two-way repeated measures ANOVA (Supplementary Table 1): * $p < 0.05$. B % of time spent in the target quadrant during 60 sec of probe test was analyzed by a two-way ANOVA with APP and PCSK9 expression as factors, and sex as covariate (See methods and Supplementary Table 1). C Occupancy plots for grouped data. The colour scale represents the average search time during time. D analysis of search strategy. Data are analyzed by chi-square test (Supplementary Table 1): * vs Wt-PCSK9^{Het}; ◦ vs Wt-PCSK9^{KO}; § 5XFAD-PCSK9^{KO}. ◦,§$p < 0.05$; *** $p < 0.0001$. Data are shown as mean ± SEM (Panels A-B). Experimental groups: Wt-PCSK9^{Het}, n = 14; Wt-PCSK9^{KO}, n = 10; 5XFAD-PCSK9^{Het}, n = 15; 5XFAD-PCSK9^{KO}, n = 12.

was not influenced by PCSK9 expression (Fig. 7 **A-F** and Supplementary Table 1 for statistical report), except for a trend toward a significant effect of PCSK9 loss on the size distribution of ThS^{+} plaques in the Nctx ((Fig. 7 **B** and Supplementary Table 1 for statistical report).

To investigate if reduced plaque area is a result of increased amyloid compaction or a consequence of a delayed amyloidosis, we further examined Aβ compaction expressed as the diffuseness index ((Area 6E10 – Area ThS) / Area 6E10) (not shown). The analysis did not demonstrate any influence of PCSK9 loss on the plaque diffuseness in both Nctx and Hip (Supplementary Table 1).

Altogether, the data demonstrated that the absence of PCSK9 induced a global reduction in amyloidosis without influencing their regional distribution and maturation.

3.2.3. *BACE1 immunoreactivity*

The BACE1, highly expressed in the CNS, has been implicated in AD and shown to be significantly increased in 10 mo 5XFAD mice (Ohno et al., 2007).

The densitometric analysis of BACE1 ir did not show any statistical differences in the ir area in the stratum lucidum (SL) of CA3, an area with very intense BACE1 labelling, between the experimental groups. In addition, the analysis of BACE1 ir thickness in SL, as a morphometric parameter, did not reveal any difference between the experimental groups (Fig. 8 **A-F**).

Furthermore, as also reported by others (Sadleir et al., 2016), we found a BACE1 ir elevation in presynaptic dystrophic neurites that surround amyloid plaques. In fact, as shown in higher magnification images, we found an increased BACE1 ir (DAB^{+} spots, brown) close to Congo Red^{+} amyloid plaques (red) in 5XFAD mice (Fig. 8 **C,D**). Given the reduced amyloidosis in 5XFAD-PCSK9^{KO} mice, we asked whether BACE1^{+} plaque-associated dystrophic neurites were also reduced in these mice. BACE1-labelled brain slices were co-labelled with Congo Red stain and the number of double positive plaques was manually counted. In line with a global reduction of amyloidosis, the quantitative analysis showed that the loss of PCSK9 induced a significant reduction in BACE1-plaque associated dystrophic neurites in Nctx; however, the ratio between the number of double positive Congo Red^{+}-BACE1^{+} plaques / total number of Congo Red^{+} plaques in 5XFAD-PCSK9^{KO} mice was

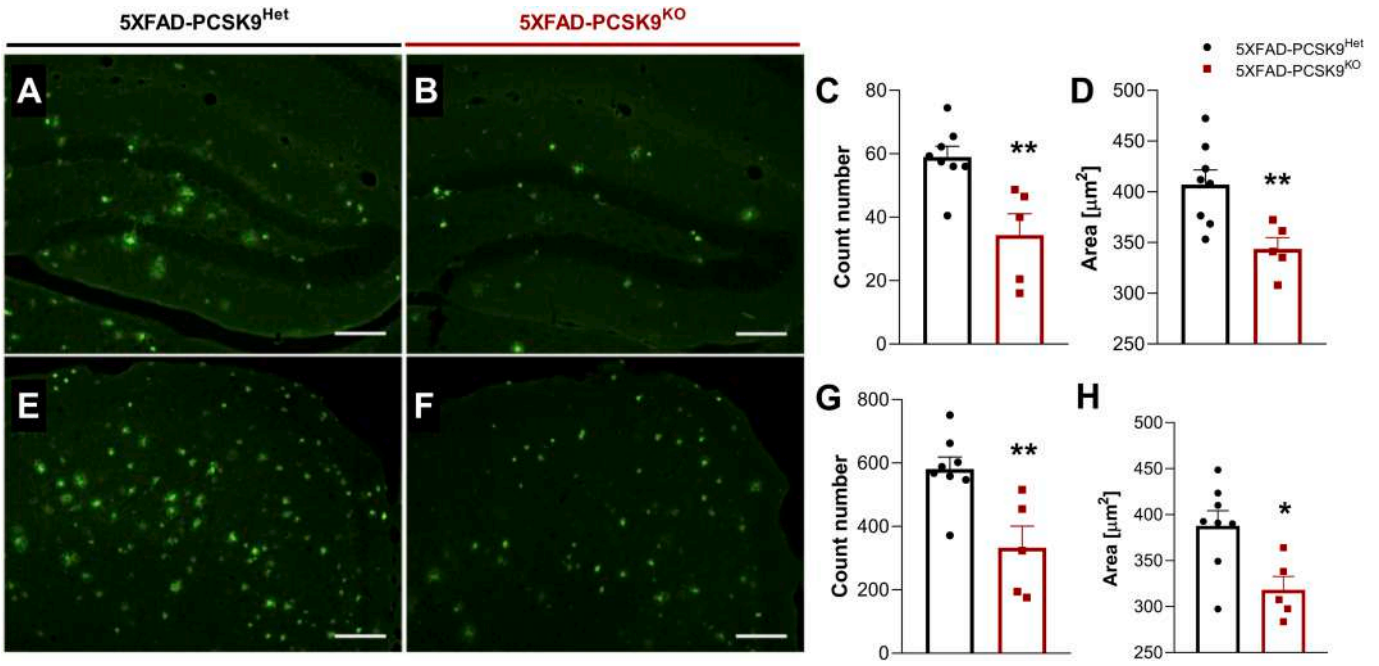

Fig. 5. Plaque deposition is reduced in 5XFAD mice in absence of PCSK9. A-B, E-F Representative images showing ThS^{+} plaque in DG (A-B) and Nctx (E-F) of 10 mo 5XFAD-PCSK9^{Het} and 5XFAD-PCSK9^{KO} mice. Scale bar = 200 µm. C-D, G-H Quantitative analysis of plaque count (C,G) and area (D,H) in DG and Nctx of 5XFAD-PCSK9^{Het} and 5XFAD-PCSK9^{KO} mice. Data are shown as mean ± SEM. Statistical analysis according to two-way ANOVA: *p < 0.05, **p < 0.01; sex was used as covariate as appropriate (See methods and Supplementary Table 1). Experimental groups: 5XFAD-PCSK9^{Het}, n = 9; 5XFAD-PCSK9^{KO}, n = 5.

comparable to that of 5XFAD-PCSK9^{Het} mice (Fig. 8 **G** and Supplementary Table 1 for detailed statistical report).

3.2.4. *Glial fibrillary acidic protein immunoreactivity*

In physiological conditions, astrocytes contribute to neuronal homeostasis in the CNS, including cholesterol supplementation to neurons. In response to various stimuli, astrocytes undergo morphological, molecular and functional changes known as astrogliosis. In this condition, these cells may contribute to neuronal damage through various mechanisms, including enhanced pro-inflammatory cytokine production. We thus analyzed the impact of PCSK9 loss on GFAP ir, a marker for astrocyte reactivity. Representative images from several brain regions, such as CC-Cg, DG hilus, CA1 and CA3 fields of Hip of the four experimental groups are shown in Fig. 9. The global semiquantitative analysis demonstrated that, compared to Ctrls, all analyzed areas are characterized by a significant increase in GFAP ir in 10 mo 5XFAD mice, that was overall counteracted by the absence of PCSK9, reaching difference statistically significant only in CC-Cg (Fig. 9 **I** and Supplementary Table 1 for detailed statistical report).

3.2.5. *Ionized calcium-binding adapter molecule 1 immunoreactivity*

Microglial cells, as the immune cells of CNS, phagocytize Aβ and apoptotic cellular debris, thus contributing to their clearance. To assess whether the reduced plaque deposition observed in 5XFAD-PCSK9^{KO} mice is associated with a decrease in neuroinflammation, we studied the reactivity of microglial cells, visualized by IBA1 ir. In Fig. 10, representative images of analyzed brain regions, such as the hippocampal hilus (**A,C,E,G**) and the sCtx (**B, D, F, H**) of experimental mice are shown. The global quantitative analysis demonstrated that the increased IBA1 ir in 5XFAD mice is counteracted by PCSK9 loss. The analysis in 5XFAD mice demonstrated a significant reduction in microgliosis in 5XFAD mice lacking PCSK9 in both DG hilar region and cortical areas (Fig. 10 **I**). Furthermore, reduced microgliosis is accompanied by a significant decrease in the number of microglial cells (not shown). Statistical analysis is detailed in Supplementary Table 1.

3.2.6. *Synaptophysin immunoreactivity*

Loss of synapses at a fine structural level and reduction in synaptic markers have been well documented in the early and late stages of AD, as well as in AD mouse models and have been shown to correlate with the extent of cognitive deficits (Wu et al., 2021). To assess whether the improved cognitive abilities and reduction of amyloid plaques in 5XFAD-PCSK9^{KO} mice in comparison with 5XFAD-PCSK9^{Het} mice are accompanied by changes at the synaptic level, we studied SYN ir as an index of synaptic integrity in the CA3 field of the hippocampus (**Supplementary** Fig. 2).

In all experimental groups, SYN ir was primarily observed in neuropil with dense labelling in dendrites. Densitometric analysis showed that the PCSK9^{KO} genotype displayed significantly increased intensity of SYN ir in stratum lucidum (SL), but not in the stratum oriens (SO) or in the stratum radiatum (SR), Interestingly, the genotype 5XFAD had no significant effect (**Supplementary** Fig. 2 **E**). No significant changes in any quantitative morphometric parameter analyzed in SL, such as area (**Supplementary** Fig. 2**F**), SYN ir length and thickness, area/thickness ratio, area/CA3 length ratio, SYN + CA3/SYN ir SL thickness, were detected despite the presence of Aβ deposits (not shown) (Supplementary Table 1 for detailed statistical report). In addition, protein quantification by western blotting analysis confirmed that SYN expression was unaffected in the Hip of experimental mice (**Supplementary** Fig. 2 **G**).

Overall, our data suggest that, at least in the present experimental conditions, the absence of PCSK9 may alter synaptic structure, as suggested by SYN ir changes, irrespectively of the presence of AD pathology.

3.2.7. *Ex-vivo analysis of neuroinflammation and lipid metabolism genes*

We preliminarily tested the expression of lipid/cholesterol metabolism-, microglial- and cytokine-related genes in B6SJL and 5XFAD mice (**Supplementary** Fig. 3). We found that most of lipid-related proteins (*Apoe, Lpl, Lrp5*), microglial factors (*P2ry12, Ifitm3, Cd11b, Cx3cr1, Cst7*) and inflammatory mediators (*Il6*, *TnfA*, *Il1B, Ccl3, Ccl6*) genes were upregulated in 5XFAD mice with only minor exceptions (*Lrp1, Cd36, Stmn1*).

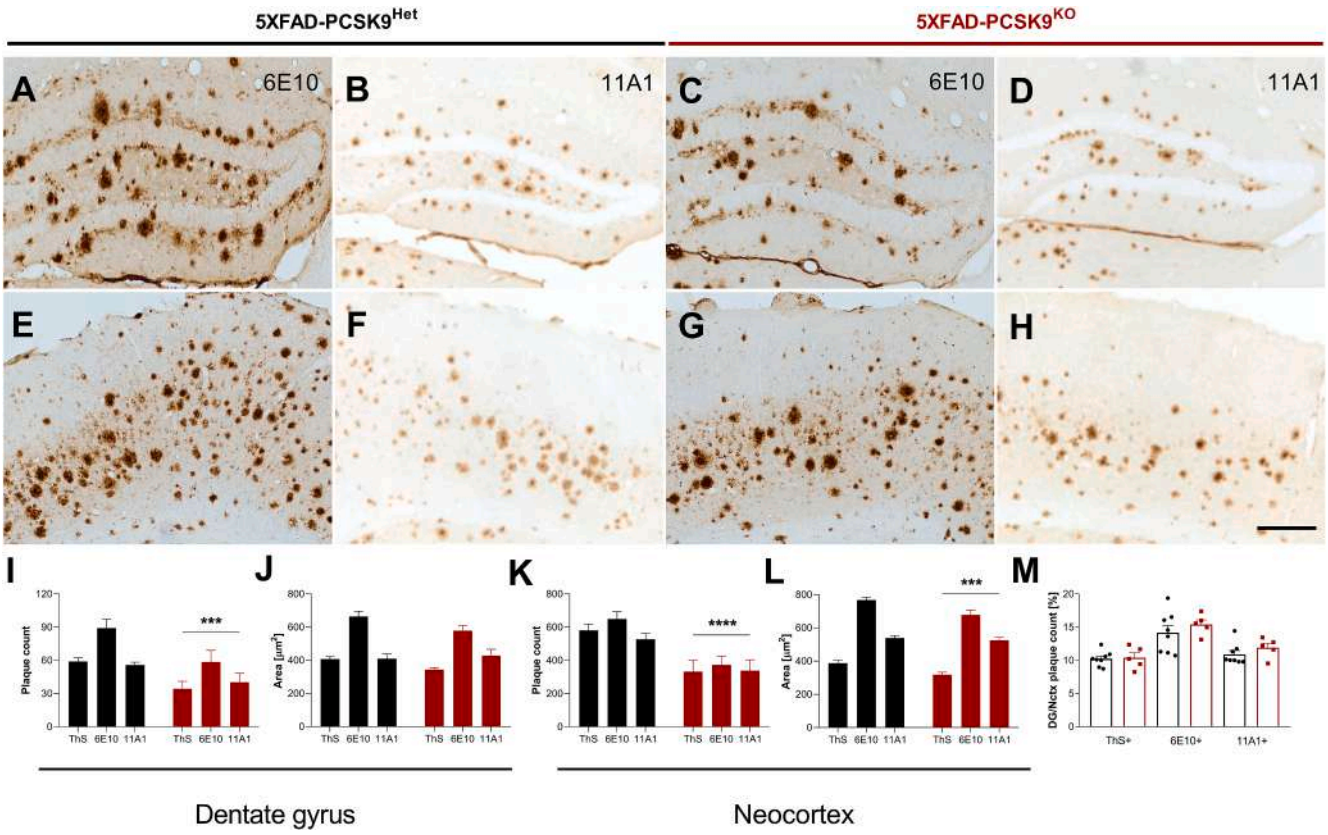

Fig. 6. Spatial distribution and quantitative characterization of differently stained plaques within cortical and hippocampal regions. A-H Representative images showing 6E10^{+} and 11A1^{+} plaque in DG and Nctx of 10 mo 5XFAD-PCSK9^{Het} (A-B; E-F) and 5XFAD-PCSK9^{KO} (C-G; G-H) mice, respectively. Scale bar = 200 μm. I-L ThS^{+}, 6E10^{+} and 11A1^{+} amyloid plaque distribution in DG and Nctx of 5XFAD-PCSK9^{Het} (black bars) and 5XFAD-PCSK9^{KO} (red bars) mice. Data are shown as mean ± SEM. Statistical analysis according to chi-square test (Supplementary Table 1): ***p < 0.001, ****p < 0.0001. M % of hippocampal/neocortical Aβ^{+} plaques in 5XFAD-PCSK9^{Het} (black bars) and 5XFAD-PCSK9^{KO} (red bars) mice. Data are shown as mean ± SEM. Statistical analysis according to two-way repeated measure ANOVA or two-way ANOVA as appropriate (See methods and Supplementary Table 1). Experimental group: 5XFAD-PCSK9^{Het}, n = 9: 5XFAD-PCSK9^{KO}, n = 5. (For interpretation of the references to colour in this figure legend, the reader is referred to the web version of this article.)

Then we analysed the expression of the above-mentioned genes in the Nctx of Ctrls and 5XFAD mice to test if the absence of PCSK9 modulates neuroinflammation and lipid metabolism gene expression (**Supplementary Fig. 4**).

As concerns lipid metabolism-related proteins, the analysis demonstrated a significant increase in *Apoe*, *Lrp5*, *Lpl* and a slight, not significant, decrease in *Cd36* expression in 5XFAD mice with no effects of PCSK9 loss; in addition, a trend towards a significant reduction in *Lrp5* expression was induced by PCSK9 loss in 5XFAD mice. *Lrp1* expression was not affected in 5XFAD mice (for the statistical report see Supplementary Table 1).

Analysis of *Stmn1*, expressed by both neurons and proliferating microglia, revealed no expression changes. Conversely, expression of microglial genes *P2ry12*, a marker of homeostatic microglia, *Cd11b* and *Cx3cr1*, as well as of *Ifitm3* and *Cst7*, identifying phagocytic/disease-associated microglia, was upregulated in 5XFAD mice regardless of PCSK9 loss (for statistical report see Supplementary Table 1).

Finally, all pro-inflammatory cytokines analyzed, *Il6*, *TnfA, Il1B*, *Ccl3* and *Ccl6,* showed a significant increase in 5XFAD mice independently of PCSK9 loss (Supplementary Table 1).

3.2.8. *Brain cholesterol and oxysterols quantification*

We finally assessed whether the absence of PCSK9 in 5XFAD mice may lead to an alteration in brain total cholesterol (TC) and oxysterols.

In a preliminary study, we observed a TC reduction by about 52 % in 5XFAD mice as compared to B6SJL controls (Supplementary Table 2), demonstrating a significant alteration in cerebral cholesterol homeostasis in 5XFAD mice. Then, we compared TC levels in our experimental mice (Table 2). We found that TC levels were similar between the mice in the Ctrl groups, irrespective of the presence or absence of PCSK9. In 5XFAD mice, a significantly lower brain TC content was detected as compared to the Ctrls. This reduction was slightly recovered by PCSK9 loss (Table 2 and Supplementary Table 1 **for statistical report**).

In parallel, we also quantified serum cholesterol TC levels in our mouse models. In a preliminary analysis, serum TC levels were shown to be similar in 5XFAD and B6SJL mice (Supplementary Table 4 **and** Supplementary Table 1 **for statistical report**). In the experimental groups, the global analysis of serum TC levels demonstrated a significant effect of 5XFAD and PCSK9 factors but no interaction; furthermore, the analysis in 5XFAD mice showed a significant effect of PCSK9 loss. (Supplementary Table 5 **and** Supplementary Table 1 for statistical report).

The most relevant oxidative bioactive metabolites of cholesterol, 24-, 25- and 27-OHC, were then quantified in the cerebral tissue and serum of the above-described animal models. In detail, we found that only 24- and 27-OHC were detectable in the brain. 5XFAD mice displayed 4-fold higher brain 27-OHC levels as compared to B6SJL controls ($p < 0.05$; Supplementary Table 3 and Supplementary Table 1 for statistical report). Instead, 24- and 27-OHC levels were comparable between the four experimental groups (Table 3). A parallel analysis of serum did not evidence significant differences in 24-, 25- and 27-OHC levels between the experimental groups (Supplementary Tables 6 and 7, see Supplementary Table 1 for statistical report).

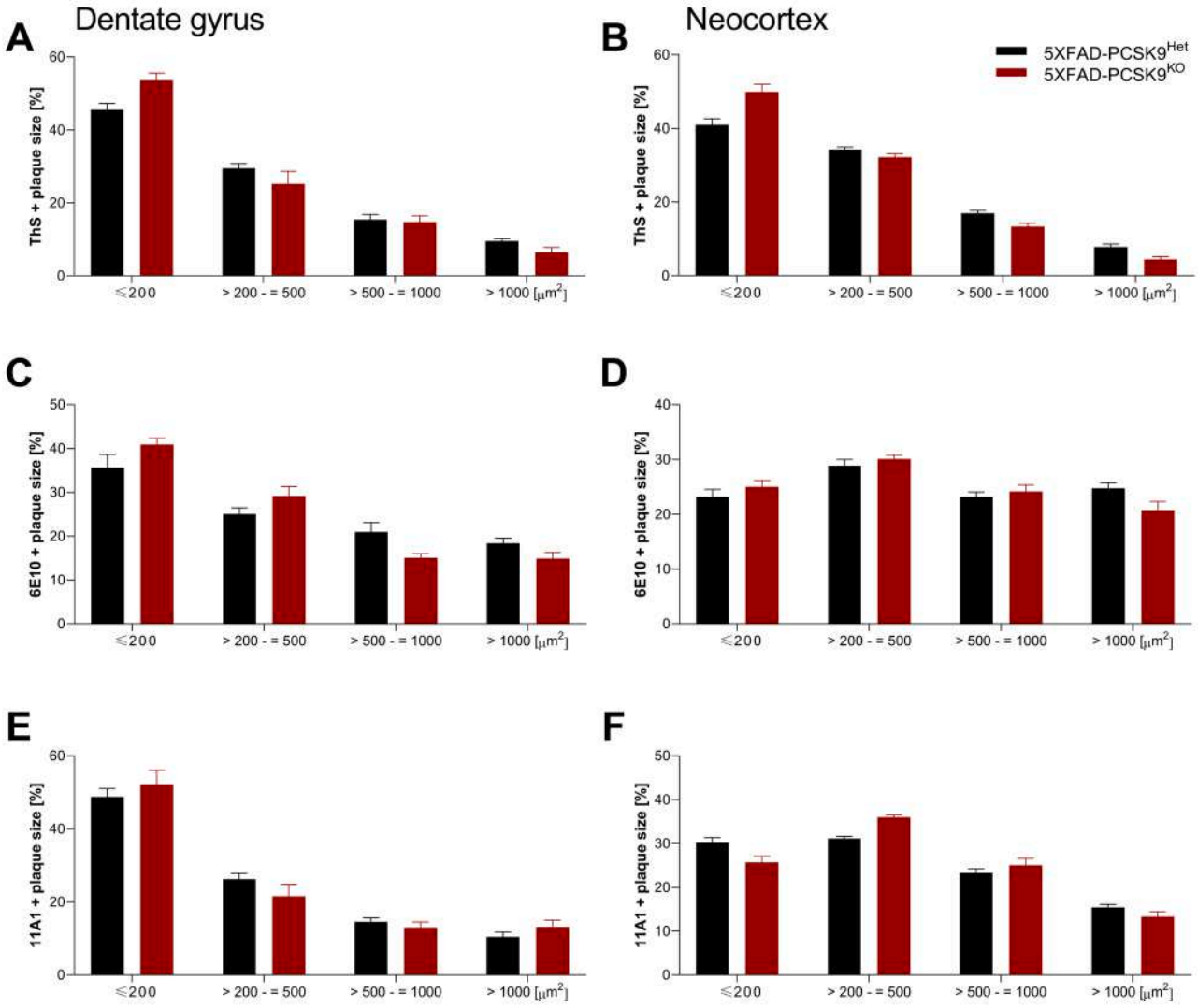

Fig. 7. Size distribution of ThS^{+}, 6E10^{+} and 11A1^{+} amyloid plaque in the hippocampal dentate gyrus (A,C,E) and neocortex (B,D,F) of 5XFAD-PCSK9^{Het} (black bars) and 5XFAD-PCSK9^{KO} (red bars) mice. Data are shown as mean ± SEM. Statistical analysis according to chi-square test (Supplementary Table 1) Experimental group: 5XFAD-PCSK9^{Het}, n = 9; 5XFAD-PCSK9^{KO}, n = 5. (For interpretation of the references to colour in this figure legend, the reader is referred to the web version of this article.)

4. Discussion

Among AD pathogenic factors, altered brain cholesterol homeostasis in CNS is a well-recognized contributor, causing oxidative stress, neuroinflammation, synaptic and neuronal dysfunction and leading to cognitive decline (McFarlane and Kedziora-Kornatowska, 2020). Recent data showed that PCSK9, a key regulator of LDLR leading to its lysosomal degradation and increasing plasma low-density lipoprotein (LDL)-cholesterol levels, is dynamically regulated and highly expressed in different neuropsychiatric disease states. However, its contribution to AD is still controversial and only little evidence is available on the beneficial effect of PCSK9 inhibition on Aβ pathology and cognitive functions. The limit of the available data is that they were obtained in animal models only partially mimicking AD phenotype (i.e., high fat-diet rats) (Abuelezz and Hendawy, 2021; Arunsak et al., 2020), or through the use of monoclonal Abs that only target peripheral PCSK9, given their inability to cross the BBB (Mazura et al., 2022).

The present study highlighted for the first time the role of PCSK9 in modulating the neuroinflammatory response, through the inhibition of several key inflammatory markers in human U373 astrocytoma cells after the exposure to Aβ fibrils **(**Figs. 1-3**)**. In addition, we reported several protective effects of the full ablation of PCSK9 in 5XFAD mice, a severe mouse model of AD, including effects on spatial learning and memory, and neuropathological outcomes, as well as on microglial density, distribution and morphology.

In detail, we clearly demonstrated that disrupted hippocampus-dependent performance of a spatial memory task in 10 mo 5XFAD mice (**Supplementary** Fig.1) was significantly improved by the absence of PCSK9 (Fig. 4). In fact, while in the initial cue-guided training period (D1-D7) all mice demonstrated a similar performance, in the second training period (D8-D13) only 5XFAD mice lacking PCSK9 were able to learn and locate the position of the hidden platform through spatially directed strategies similarly to Ctrls. These data are in accordance with those recently obtained by others in the high-fat cholesterol diet (HFCD)- a model of AD-like condition in rats (Abuelezz and Hendawy, 2021) and in 6 mo 5XFAD mice (Mazura et al., 2022) after systemic PCSK9 inhibition through monoclonal anti-PCSK9 Ab injection. Furthermore, here we add new insights into the role of PCSK9 on

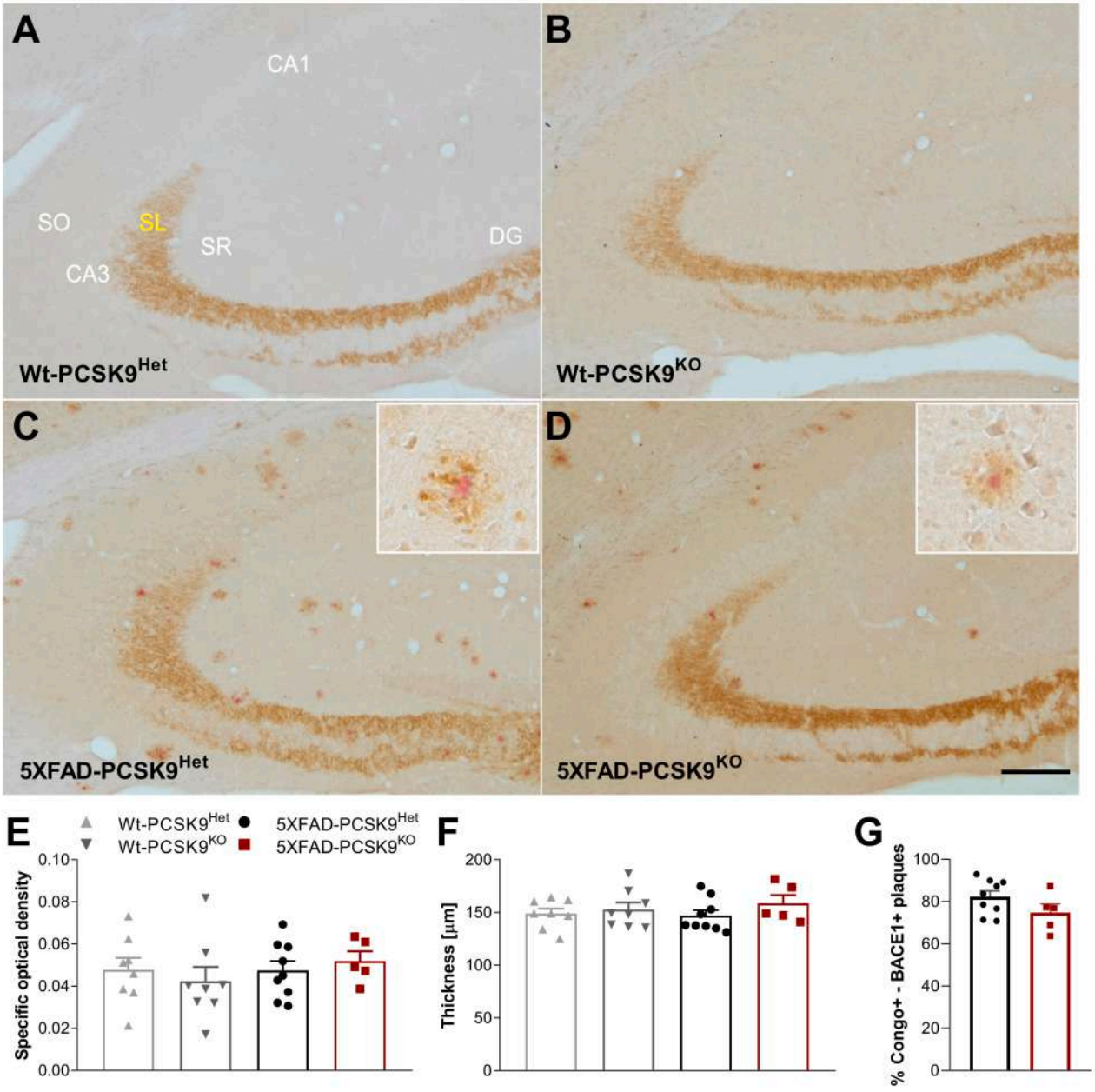

Fig. 8. Representative photomicrographs of CA3 field of hippocampus of 10 mo Wt-PCSK9^{Het} (light grey bars), Wt-PCSK9^{KO} (dark grey bars), 5XFAD-PCSK9^{Het} (black bars) and 5XFAD-PCSK9^{KO} (red bars) mice showing immunoreactivity for BACE1 and Congo Redstained amyloid plaques (A-D). Scale bar = 200 μm. E-F Densitometric analysis of BACE1 ir in hippocampal stratum lucidum (SL) of CA3 field by analyzing specific optical area (E) and BACE1 ir thickness (F). Data are shown as mean ± SEM and compared by two-way ANOVA test (Supplementary Table 1). G % of co-stained Congo Red-BACE1^{+} plaques in Nctx of 5XFAD-PCSK9^{Het} (black bars) and 5XFAD-PCSK9^{KO} (red bars). Data are shown as mean ± SEM and compared by chi-square test (Supplementary Table 1).Experimental groups: Wt-PCSK9^{Het}, n = 8; Wt-PCSK9^{KO}, n = 8; 5XFAD-PCSK9^{Het}, n = 10; 5XFAD-PCSK9^{KO}, n = 5.Abbreviations: DG = dentate gyrus; CA3 = cornu Ammonis 3; CA1 = cornu Ammonis 1; SR = Stratum Radiatum; SL = Stratum Lucidum; SO = Stratum Oriens. (For interpretation of the references to colour in this figure legend, the reader is referred to the web version of this article.)

hippocampal-dependent cognitive decline. In fact, the inability to form and retain new memories is among the most precocious and common features of human AD and such deficits are dependent on the entorhinal cortex, perforant pathway, and hippocampus. We demonstrated that PCSK9 loss improves hippocampal-dependent memory impairment in 10 mo 5XFAD, and specifically it ameliorates spatial abilities (learning curve) as well as retention of spatial reference memory (probe test). Finally, since recent data revealed an increased expression of PCSK9 in AD (Picard et al., 2019), we can speculate that the observed changes are a direct consequence of PCSK9 loss in the CNS, although we cannot exclude an indirect influence of peripheral PCSK9 loss (Mazura et al., 2022). Taken together, these data demonstrated that the inhibition of PCSK9 is able to preserve hippocampal-dependent learning abilities and memory in AD animal models.

In agreement with the data on cognitive improvement, also Aβ burden was shown to be influenced by PCSK9. In fact, PCSK9 loss induced a marked reduction in both count and area of ThS^{+} and 6E10^{+} plaques and in count of 11A1^{+} plaques in corticohippocampal regions of

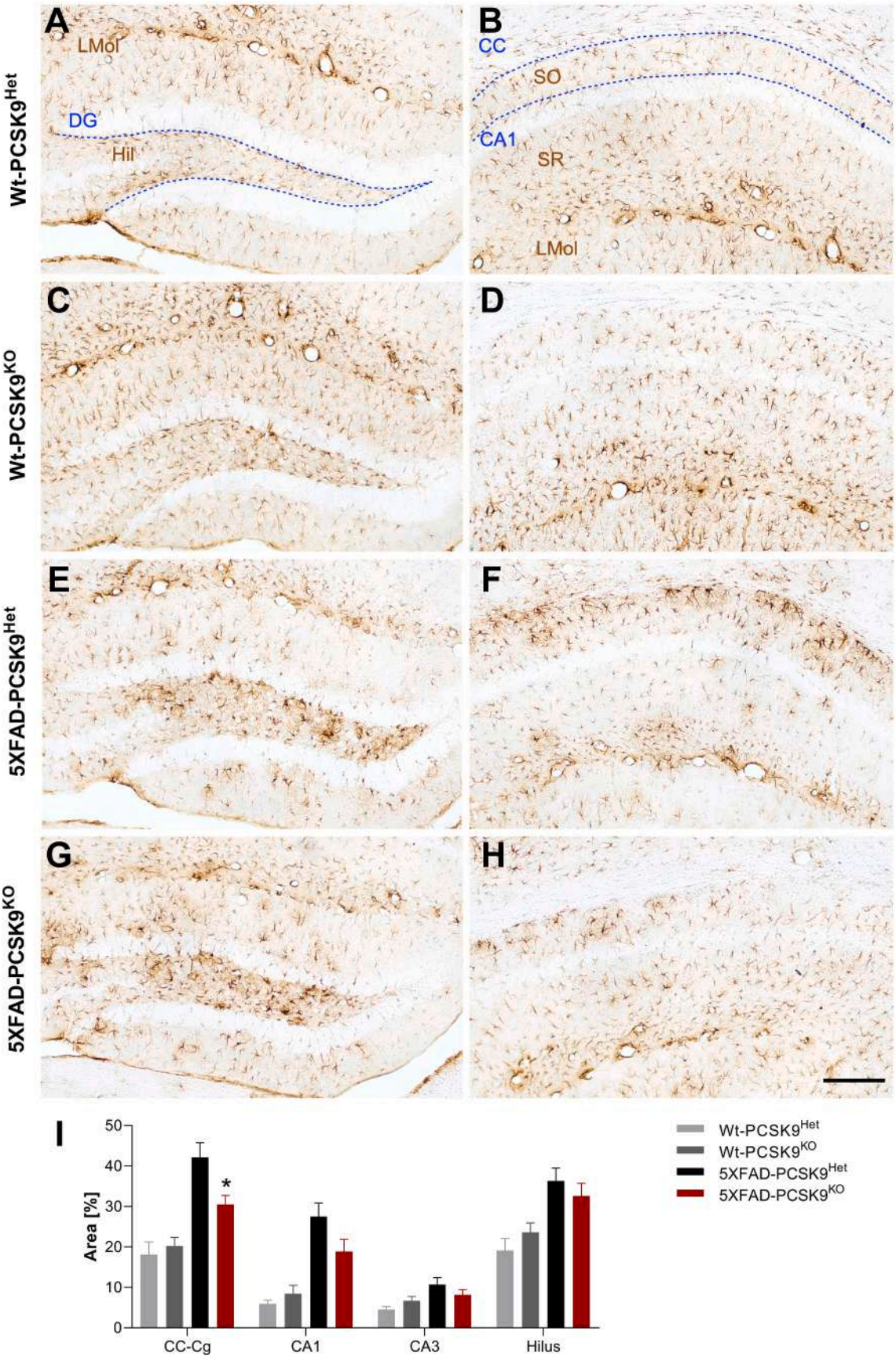

(caption on next page)

Fig. 9. Astrocyte reactivity in AD mice is influenced by PCSK9 loss. A-H. Representative photomicrographs of dentate gyrus (A, C, E, G) and CA1 (B, D, F, H) fields of hippocampus of 10 mo Wt-PCSK9^{Het} (A-B and light grey bars), Wt-PCSK9^{KO} (C-D and dark grey bars), 5XFAD-PCSK9^{Het} (E-F and black bars) and 5XFAD-PCSK9^{KO} (G-H and red bars) mice showing GFAP ir. Scale bar = 200 μm. I Quantitative analysis of GFAP ir in CC-Cg, Hilus, CA1, CA3 fields of Hipp of 10 mo mice. Data are shown as mean ± SEM; GFAP ir in different brain areas was compared by two-way repeated measure ANOVA (Supplementary Table 1). The analysis in 5XFAD mice was performed by one-way ANOVA (Supplementary Table 3): * $p < 0.05$; Experimental groups: Wt-PCSK9^{Het}, n = 5–6; Wt-PCSK9^{KO}, n = 5–7; 5XFAD-PCSK9^{Het}, n = 9; 5XFAD-PCSK9^{KO}, n = 5). Abbreviations: DG = dentate gyrus; LMol = stratum lacunosum-moleculare; Hil = hilus; CC-Cg = corpus callosum-cingulate cortex; CA1 = cornu Ammonis 1; SR = Stratum Radiatum; SL = Stratum Lucidum; SO = Stratum Oriens. (For interpretation of the references to colour in this figure legend, the reader is referred to the web version of this article.)

5XFAD mice (Figs. 5-6), with no effects either in the regional distribution or in plaque size distribution of amyloid plaques (Figs. 6 and 7). Supported by recent studies (Abuelezz and Hendawy, 2021; Apaijai et al., 2019; Arunsak et al., 2020), these results suggest a role of PCSK9 in promoting plaque formation since its inhibition attenuates Aβ aggregation. This effect is unlikely to depend on changes in either global BACE1 expression or its accumulation in *peri*-plaque dystrophic neurites (Fig. 8). In fact, whereas the role of PCSK9 in modulating BACE1 activity is still controversial, showing an increase or decrease in different experimental conditions (Liu et al., 2010), here we clearly demonstrated that % of Congo Red^{+} - BACE1^{+} plaques was comparable between 5XFAD mice with or without PCSK9 (Fig. 8).

Emerging evidence has also implicated PCSK9 in neuroinflammation, namely through a role in coordinating the induction of NF-κB pathway and the activation of astrocytes and microglia (Abuelezz and Hendawy, 2021; Apaijai et al., 2019). Our *in vitro* data, though not obtained in primary astrocytes, demonstrated that recombinant PCSK9 exacerbated the Aβ fibrils-mediated induction of proinflammatory cytokines in U373 astrocytoma cell line (Figs. 1-3). Accordingly, the loss of PCSK9 in 5XFAD mice decreased microglial reactivity, a hallmark of inflammation in the brain, in corticohippocampal regions to the levels of Ctrls, in terms of global IBA1 ir and number of microglial cells. This result is consistent with recent studies showing reduced brain damage and decreased microglial reactivity in ischemic rats treated with PCSK9 inhibitors (Apaijai et al., 2019), as well as a reduced activation of human peripheral blood monocytes induced by PCSK9 inhibition (Liu and Frostegard, 2018). However, the marked increase in the cortical expression of homeostatic genes, such as *P2ry12*, *Cd11b* and *Cx3cr1*, as well as in the phagocytic/disease-associated genes of microglia, such as *Ifitm3* and *Cst7*, observed in 10 mo 5XFAD mice was not modulated by PCSK9 loss (Supplementary Figs. 3 and 4). These data, though limited to an analysis of transcripts, let us hypothesize that reduced amyloid plaque deposition in the absence of PCSK9 is not a consequence of accelerated Aβ phagocytosis. In this view, increased expression of *Cd36* has been associated with an increased Aβ1–42 uptake in the brain and lowered Aβ plaque burden in the Hip of 5XFAD mice (Koronyo et al., 2015; Koronyo-Hamaoui et al., 2020; Lucin et al., 2013). However, our analysis revealed only a minor decrease in *Cd36* expression dependent on AD-like pathology but not PCSK9 loss. The lack of effect on *Cd36* was also confirmed by our *in vitro* experiments in astrocytes. Since gene expression analysis has been conducted on the whole cerebral cortex, the most Aβ–affected brain region in 5XFAD mice, we cannot exclude that PCSK9 loss may induce cell type- and/or brain area-specific alterations that are overlooked with our technical approach.

Despite the fact that PCSK9 loss modulates microglial reactivity, on the other hand its absence did not cause a marked global reduction in GFAP ir, an index of astrogliosis, with the exceptions of CC-Cg (Fig. 9). Since GFAP ir does not label all astrocytic populations, especially in areas such as cerebral cortex, our data do not exclude that PCSK9 loss may have a more pervasive, protective effect on other astrocytic populations. Additionally, it is known that GFAP^{+} astrocytes contain subpopulations with different functional roles, such as A1 neurotoxic astrocytes, the major astrocytic subtype that mediates astrocytic toxicity in AD (Lau et al., 2021). Further studies with A1-specific markers may show alterations in astrocytic subpopulations that have been overlooked in the present analysis.

Finally, reduced brain cholesterol levels in 10 mo 5XFAD mice (Supplementary Table 2) were partially restored by PCSK9 loss (Table 2). In addition, our results indicated an absence of changes in oxysterols (Table 3), thus suggesting that the ameliorated cognitive performance, reduced amyloidosis and neuroinflammation caused by PCSK9 deletion could only partially be explained by a restoration of lipid homeostasis. The lack of prominent differences in brain cholesterol across the PCSK9 genotypes may be interpreted in light of a possible interfering effect of PCSK9 specifically on the brain cholesterol flux from astrocytes to neurons, that we previously hypothesized, but not necessarily accompanied by overall changes in total brain content. In this regard, future studies investigating the differential effect of PCSK9 loss on cholesterol content in primary astrocytes and neurons will be of great interest.

Accordingly, also the expression of lipid-related genes was unaffected by PCSK9 loss, with minor exceptions. In fact, both *Apoe* and *Lpl* were increased in 5XFAD mice without any interference by PCSK9. For the reasons mentioned above, we cannot exclude that cell-specific changes occur in 5XFAD in the absence of PCSK9.

5. Conclusion

Present data strongly evidence a protective role of PCSK9 genetic deletion against Aβ pathology, neuroinflammation and cognitive decline in a severe mouse model of AD, thus putting the premises to identify PCSK9 as a pharmacological target for development of novel therapeutic strategies for AD, for which no treatment is yet available.

Funding

Ths research was funded by: Amgen's PSCK9 Competitive Grant Program 2018, grant number 9,406,917 (to FB), the National Recovery and Resilience Plan (NRRP), M4 C2 Investment 1.3— Project code PE0000006 (MNESYS to FB), the MIUR Dipartimenti di Eccellenza 2018–2022 (to AV, MB, ED, MZ) and 2023–2027 (to BP, FZ, GR. LE, IZ, FB). BP is supported by funding obtained under the National Recovery and Resilience Plan (NRRP), M4 C2 Investment 1.3— Project code PE0000006 (MNESYS).

7. Consent for publication

All authors have read and agreed to the published version of the manuscript.

Competing interests

Part of this research was funded by Amgen's PSCK9 Competitive Grant Program 2018, grant number 9,406,917 to Prof. F. Bernini.

CRediT authorship contribution statement

Antonietta Vilella: Investigation, Formal analysis, Data curation, Methodology, Supervision, Writing – original draft, Writing – review & editing. **Martina Bodria:** Investigation. **Bianca Papotti:** Investigation, Formal analysis, Methodology, Writing – review & editing. **Francesca Zimetti:** Investigation, Conceptualization, Data curation, Supervision, Writing – original draft, Writing – review & editing. **Giulia Remaggi:** Investigation, Formal analysis. **Lisa Elviri:** Investigation, Formal

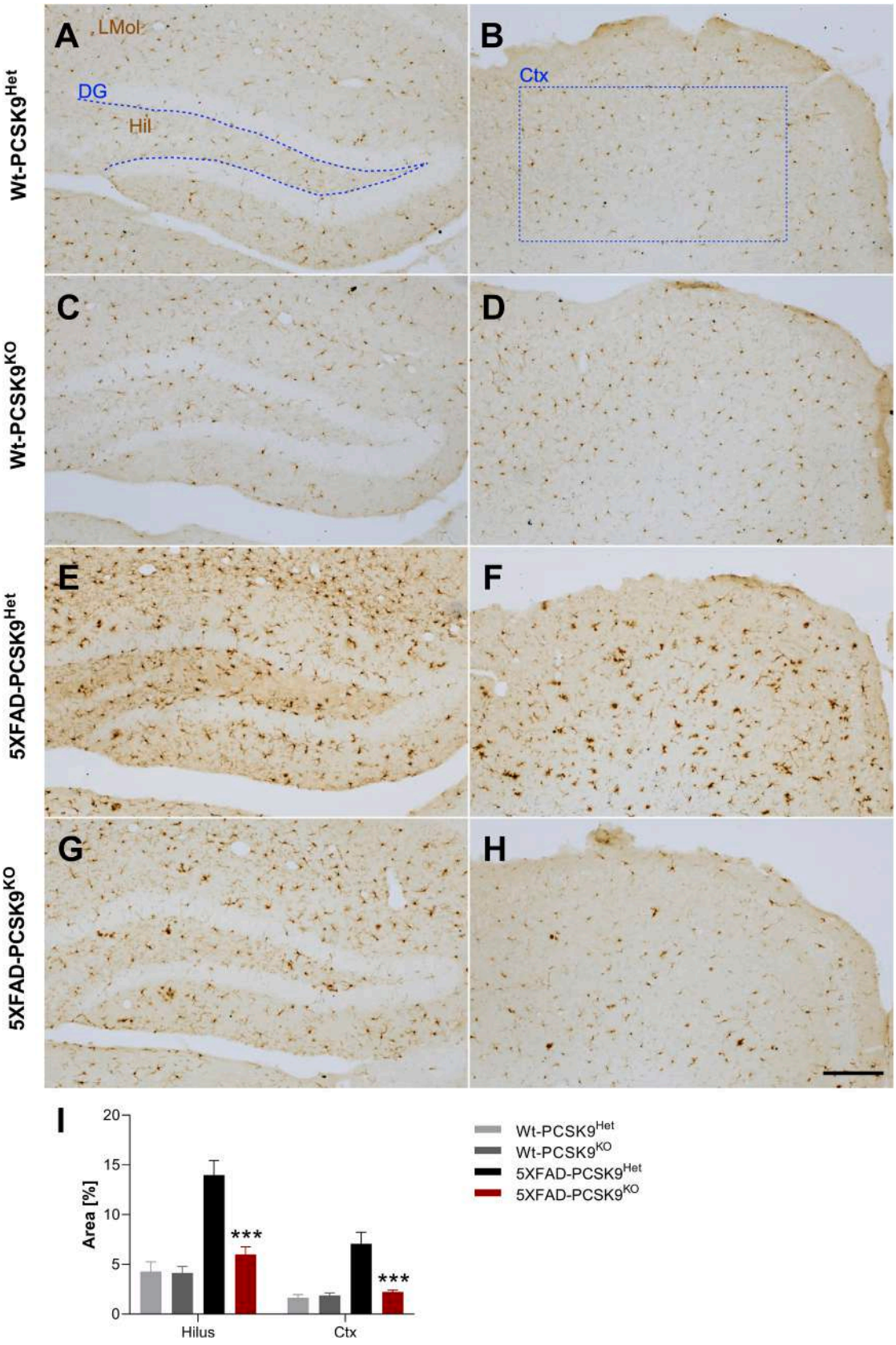

Fig. 10. The loss of PCSK9 significantly reduced hippocampal and cortical microgliosis in AD mice. A-H Representative images of brain slices showing IBA1^{+} microglial cells in the hilus of dentate gyrus (A,C,E,G) and cerebral cortex (B,D,F,H) of Wt (A-D) and 5XFAD (E-H) mice. Scale bar = 200 μm. I-J Quantitative analysis of microgliosis in Ctx and hilar region of Hipp. Data are shown as mean ± SEM. Statistical analysis according to two-way repeated measure ANOVA. The analysis was performed in 5XFAD mice by one-way ANOVA (Supplementary Table 1): ***$p < 0.001$. Experimental groups: Wt-PCSK9^{Het}, n = 6; Wt-PCSK9^{KO}, n = 6; 5XFAD-PCSK9^{Het}, n = 5; 5XFAD-PCSK9^{KO}, n = 5). Abbreviations: DG = dentate gyrus; LMol = stratum lacunosum-moleculare; Hil = hilus; Ctx = cerebral cortex.

Table 2
Brain total cholesterol levels of 10 mo Wt-PCSK9^{Het}, Wt-PCSK9^{KO}, 5XFAD-PCSK9^{Het} and 5XFAD-PCSK9^{KO} mice.

	μg/mg cerebral tissue
Wt-PCSK9^{Het}	1.86 ± 0.17
Wt-PCSK9^{KO}	1.35 ± 0.24
5XFAD-PCSK9^{Het}	0.95 ± 0.13
5XFAD-PCSK9^{KO}	1.18 ± 0.17

Brain cholesterol levels are expressed as (μg cholesterol/mg of cerebral tissue). Data are shown as mean ± SEM. Wt-PCSK9^{Het} n = 12; Wt-PCSK9^{KO} n = 10; 5XFAD-PCSK9^{Het} n = 11; 5XFAD-PCSK9^{KO} n = 11. Statistical analysis according to two-way ANOVA. (Supplementary Table 1). A value of $p < 0.05$ was considered statistically significant.

Table 3
Brain hydroxysterols levels of 10 mo Wt-PCSK9^{Het}, Wt-PCSK9^{KO}, 5XFAD-PCSK9^{Het} and 5XFAD-PCSK9^{KO}.

	24-OHC (ng/ml)	25-OHC (ng/ml)	27-OHC (ng/ml)
Wt-PCSK9^{Het}	2.67 ± 0.24	n.d.	2.10 ± 0.22
Wt-PCSK9^{KO}	3.08 ± 0.24	n.d.	2.32 ± 0.58
5XFAD-PCSK9^{Het}	3.45 ± 0.46	n.d.	1.95 ± 0.57
5XFAD-PCSK9^{KO}	2.87 ± 0.53	n.d.	1.86 ± 0.36

Brain hydroxysterols are expressed as (ng hydroxysterols/mg cerebral tissue). Data are shown as mean ± SEM. Wt-PCSK9^{Het} n = 14; Wt-PCSK9^{KO} n = 10; 5XFAD-PCSK9^{Het} n = 12; 5XFAD-PCSK9^{KO} n = 12. Statistical analysis according to two-way ANOVA (Supplementary Table 1). A value of $p < 0.05$ was considered statistically significant. n.d: not detectable.

analysis. **Nicola Ferri:** Conceptualization, Formal analysis, Writing – original draft. **Maria Giovanna Lupo:** Formal analysis. **Giovanni Panighel:** Formal analysis. **Eleonora Daini:** Investigation. **Eleonora Vandini:** Investigation. **Daniela Giuliani:** Formal analysis. **Franco Bernini:** Conceptualization, Funding acquisition, Supervision, Writing – review & editing.

Declaration of Competing Interest

The authors declare that they have no known competing financial interests or personal relationships that could have appeared to influence the work reported in this paper.

Data availability

Data will be made available on request.

Appendix A. Supplementary data

Supplementary data to this article can be found online at https://doi.org/10.1016/j.bbi.2023.11.008.

References

Abuelezz, S.A., Hendawy, N., 2021. HMGB1/RAGE/TLR4 axis and glutamate as novel targets for PCSK9 inhibitor in high fat cholesterol diet induced cognitive impairment and amyloidosis. Life Sci. 273, 119310.

Adorni, M.P., Ruscica, M., Ferri, N., Bernini, F., Zimetti, F., 2019. Proprotein Convertase Subtilisin/Kexin Type 9, Brain Cholesterol Homeostasis and Potential Implication for Alzheimer's Disease. Front. Aging Neurosci. 11, 120.

Almolda, B., de Labra, C., Barrera, I., Gruart, A., Delgado-Garcia, J.M., Villacampa, N., Vilella, A., Hofer, M.J., Hidalgo, J., Campbell, I.L., Gonzalez, B., Castellano, B., 2015. Alterations in microglial phenotype and hippocampal neuronal function in transgenic mice with astrocyte-targeted production of interleukin-10. Brain Behav. Immun. 45, 80–97.

Apaijai, N., Moisescu, D.M., Palee, S., McSweeney, C.M., Saiyasit, N., Maneechote, C., Boonnag, C., Chattipakorn, N., Chattipakorn, S.C., 2019. Pretreatment With PCSK9 Inhibitor Protects the Brain Against Cardiac Ischemia/Reperfusion Injury Through a Reduction of Neuronal Inflammation and Amyloid Beta Aggregation. J. Am. Heart Assoc. 8, e010838.

Arunsak, B., Pratchayasakul, W., Amput, P., Chattipakorn, K., Tosukhowong, T., Kerdphoo, S., Jaiwongkum, T., Thonusin, C., Palee, S., Chattipakorn, N., Chattipakorn, S.C., 2020. Proprotein convertase subtilisin/kexin type 9 (PCSK9) inhibitor exerts greater efficacy than atorvastatin on improvement of brain function and cognition in obese rats. Arch. Biochem. Biophys. 689, 108470.

Badimon, L., Luquero, A., Crespo, J., Pena, E., Borrell-Pages, M., 2021. PCSK9 and LRP5 in macrophage lipid internalization and inflammation. Cardiovasc. Res. 117, 2054–2068.

Bellenguez, C., Kucukali, F., Jansen, I.E., Kleineidam, L., Moreno-Grau, S., Amin, N., Naj, A.C., Campos-Martin, R., Grenier-Boley, B., Andrade, V., Holmans, P.A., Boland, A., Damotte, V., van der Lee, S.J., Costa, M.R., Kuulasmaa, T., Yang, Q., De Rojas, I., Bis, J.C., Yaqub, A., Prokic, I., Chapuis, J., Ahmad, S., Giedraitis, V., Aarsland, D., Garcia-Gonzalez, P., Abdelnour, C., Alarcon-Martin, E., Alcolea, D., Alegret, M., Alvarez, I., Alvarez, V., Armstrong, N.J., Tsolaki, A., Antunez, C., Appollonio, I., Arcaro, M., Archetti, S., Pastor, A.A., Arosio, B., Athanasiu, L., Bailly, H., Banaj, N., Baquero, M., Barral, S., Beiser, A., Pastor, A.B., Below, J.E., Benchek, P., Benussi, L., Berr, C., Besse, C., Bessi, V., Binetti, G., Bizarro, A., Blesa, R., Boada, M., Boerwinkle, E., Borroni, B., Boschi, S., Bossu, P., Brathen, G., Bressler, J., Bresner, C., Brodaty, H., Brookes, K.J., Brusco, L.I., Buiza-Rueda, D., Burger, K., Burholt, V., Bush, W.S., Calero, M., Cantwell, L.B., Chene, G., Chung, J., Cuccaro, M.L., Cecchetti, R., Cervera-Carles, L., Charbonnier, C., Chen, H.H., Chillotti, C., Ciccone, S., Claassen, J.A.H.R., Clark, C., Conti, E., Corma-Gomez, A., Costantini, E., Custodero, C., Daian, D., Dalmasso, M.C., Daniele, A., Dardiotis, E., Dartigues, J.F., de Deyn, P.P., Lopes, K.D., De Witte, L.D., Debette, S., Deckert, J., del Ser, T., Denning, N., Destefano, A., Dichgans, M., Diehl-Schmid, J., Diez-Fairen, M., Rossi, P.D., Djurovic, S., Duron, E., Duzel, E., Dufouil, C., Eiriksdottir, G., Engelborghs, S., Escott-Price, V., Espinosa, A., Ewers, M., Faber, K.M., Fabrizio, T., Nielsen, S.F., Fardo, D.W., Farotti, L., Fenoglio, C., Fernandez-Fuertes, M., Ferrari, R., Ferreira, C.B., Ferri, E., Fin, B., Fischer, P., Fladby, T., Fliessbach, K., Fongang, B., Fornage, M., Fortea, J., Foroud, T.M., Fostinelli, S., Fox, N.C., Franco-Macias, E., Bullido, M.J., Frank-Garcia, A., Froelich, L., Fulton-Howard, B., Galimberti, D., Garcia-Alberca, J.M., Garcia-Madrona, S., Garcia-Ribas, G., Ghidoni, R., Giegling, I., Giorgio, G., Goate, A.M., Goldhardt, O., Gomez-Fonseca, D., Gonzalez-Perez, A., Graff, C., Grande, G., Green, E., Grimmer, T., Grunblatt, E., Grunin, M., Gudnason, V., Guetta-Baranes, T., Haapasalo, A., Hadjigeorgiou, G., Haines, J.L., Hamilton-Nelson, K.L., Hampel, H., Hanon, O., Hardy, J., Hartmann, A. M., Hausner, L., Harwood, J., Heilmann-Heimbach, S., Helisalmi, S., Heneka, M.T., Hernandez, I., Herrmann, M.J., Hoffmann, P., Holmes, C., Holstege, H., Vilas, R.H., Hulsman, M., Humphrey, J., Biessels, G.J., Jian, X.Q., Johansson, C., Jun, G.R., Kastumata, Y., Kauwe, J., Kehoe, P.G., Kilander, L., Stahlbom, A.K., Kivipelto, M., Koivisto, A., Kornhuber, J., Kosmidis, M.H., Kukull, W.A., Kuksa, P.P., Kunkle, B.W., Kuzma, A.B., Lage, C., Laukka, E.J., Launer, L., Lauria, A., Lee, C.Y., Lehtisalo, J., Lerch, O., Lleo, A., Longstreth, W., Lopez, O., de Munain, A.L., Love, S., Lowemark, M., Luckcuck, L., Lunetta, K.L., Ma, Y.Y., Macias, J., Macleod, C.A., Maier, W., Mangialasche, F., Spallazzi, M., Marquie, M., Marshall, R., Martin, E.R., Montes, A.M., Rodriguez, C.M., Masullo, C., Mayeux, R., Mead, S., Mecocci, P., Medina, M., Meggy, A., Mehrabian, S., Mendoza, S., Menendez-Gonzalez, M., Mir, P., Moebus, S., Mol, M., Molina-Porcel, L., Montrreal, L., Morelli, L., Moreno, F., Morgan, K., Mosley, T., Nothen, M.M., Muchnik, C., Mukherjee, S., Nacmias, B., Ngandu, T., Nicolas, G., Nordestgaard, B.G., Olaso, R., Orellana, A., Orsini, M., Ortega, G., Padovani, A., Paolo, C., Papenberg, G., Parnetti, L., Pasquier, F., Pastor, P., Peloso, G., Perez-Cordon, A., Perez-Tur, J., Pericard, P., Peters, O., Pijnenburg, Y.A.L., Pineda, J.A., Pinol-Ripoll, G., Pisanu, L., Polak, T., Popp, J., Posthuma, D., Priller, J., Puerta, R., Quenez, O., Quintela, I., Thomassen, J.Q., Rabano, A., Rainero, I., Rajabli, F., Ramakers, I., Real, L.M., Reinders, M.J.T., Reitz, C., Reyes-Dumeyer, D., Ridge, P., Riedel-Heller, S., Riederer, P., Roberto, N., Rodriguez-Rodriguez, E., Rongve, A., Allende, I.R., Rosende-Roca, M., Royo, J.L., Rubino, E., Rujescu, D., Saez, M.E., Sakka, P., Saltvedt, I., Sanchez-Arjona, M.B., Sanchez-Garcia, F., Juan, P.S., Sanchez-Valle, R., Sando, S.B., Sarnowski, C., Satizabal, C.L., Scamosci, M., Scarmeas, N., Scarpini, E., Scheltens, P., Scherbaum, N., Scherer, M., Schmid, M., Schneider, A., Schott, J.M., Selbaek, G., Seripa, D., Serrano, M., Sha, J., Shadrin, A.A., Skrobot, O., Slifer, S., Snijders, G.J.L., Soininen, H., Solfrizzi, V., Solomon, A., Song, Y., Sorbi, S., Sotolongo-Grau, O., Spalletta, G., Spottke, A., Squassina, A., Stordal, E., Tartan, J.P., Tarraga, L., Tesi, N., Thalamuthu, A., Thomas, T., Tosto, G., Traykov, L., Tremolizzo, L., Tybjaeg-Hansen, A., Uitterlinden, A., Ullgren, A., Ulstein, I., Valero, S., Valladares, O., Van Broeckhoven, C., Vance, J., Vardarajan, B.N., van der Lugt, A., Van Dongen, J., van Rooij, J., van Swieten, J., Vandenberghe, R., Verhey, F., Vidal, J.S., Vogelgsang, J., Vyhnalek, M., Wagner, M., Wallon, D., Wang, L.S., Wang, R.Q., Weinhold, L., Wiltfang, J., Windle, G., Woods, B., Yannakoulia, M., Zare, H., Zhao, Y., Zhang, X.L., Zhu, C.C., Zulaica, M., Farrer, L.A., Psaty, B.M., Ghanbari, M., Raj, T., Sachdev, P., Mather, K., Jessen, F., Ikram, M.A., de Mendonca, A., Hort, J., Tsolaki, M., Pericak-Vance, M.A., Amouyel, P., Williams, J., Frikke-Schmidt, R., Clarimon, J., Deleuze, J. F., Rossi, G., Seshadri, S., Andreassen, O.A., Ingelsson, M., Hiltunen, M., Sleegers, K., Schellenberg, G.D., van Duijn, C.M., Sims, R., van der Flier, W.M., Ruiz, A., Ramirez, A., Lambert, J.C., 2022. EADB, ACE, G., DEGESCO, EADI, GERAD, Demgene, FinnGen, ADGC, CHARGE, New insights into the genetic etiology of Alzheimer's disease and related dementias. Nat. Genet. 54, 412-+.

Benn, M., Nordestgaard, B.G., Frikke-Schmidt, R., Tybjaerg-Hansen, A., 2017. Low LDL cholesterol, PCSK9 and HMGCR genetic variation, and risk of Alzheimer's disease and Parkinson's disease: Mendelian randomisation study. BMJ 357, j1648.

Bingham, B., Shen, R., Kotnis, S., Lo, C.F., Ozenberger, B.A., Ghosh, N., Kennedy, J.D., Jacobsen, J.S., Grenier, J.M., DiStefano, P.S., Chiang, L.W., Wood, A., 2006. Proapoptotic effects of NARC 1 (= PCSK9), the gene encoding a novel serine proteinase. Cytometry A 69, 1123–1131.

Borah, K., Rickman, O.J., Voutsina, N., Ampong, I., Gao, D., Baple, E.L., Dias, I.H., Crosby, A.H., Griffiths, H.R., 2020. A quantitative LC-MS/MS method for analysis of mitochondrial -specific oxysterol metabolism. Redox Biol. 36, 101595.

Burns, S., Selman, A., Sehar, U., Rawat, P., Reddy, A.P., Reddy, P.H., 2022. Therapeutics of Alzheimer's Disease: Recent Developments. Antioxidants (Basel) 11.

Courtemanche, H., Bigot, E., Pichelin, M., Guyomarch, B., Boutoleau-Bretonniere, C., Le May, C., Derkinderen, P., Cariou, B., 2018. PCSK9 Concentrations in Cerebrospinal Fluid Are Not Specifically Increased in Alzheimer's Disease. J. Alzheimers Dis. 62, 1519–1525.

Daini, E., Secco, V., Liao, W., Zoli, M., Vilella, A., 2021. A regional and cellular analysis of the early intracellular and extracellular accumulation of Abeta in the brain of 5XFAD mice. Neurosci. Lett. 754, 135869.

de Rojas, I., Moreno-Grau, S., Tesi, N., Grenier-Boley, B., Andrade, V., Jansen, I.E., Pedersen, N.L., Stringa, N., Zettergren, A., Hernandez, I., Montrreal, L., Antunez, C., Antonell, A., Tankard, R.M., Bis, J.C., Sims, R., Bellenguez, C., Quintela, I., Gonzalez-Perez, A., Calero, M., Franco-Macias, E., Macias, J., Blesa, R., Cervera-Carles, L., Menendez-Gonzalez, M., Frank-Garcia, A., Royo, J.L., Moreno, F., Huerto Vilas, R., Baquero, M., Diez-Fairen, M., Lage, C., Garcia-Madrona, S., Garcia-Gonzalez, P., Alarcon-Martin, E., Valero, S., Sotolongo-Grau, O., Ullgren, A., Naj, A.C., Lemstra, A. W., Benaque, A., Perez-Cordon, A., Benussi, A., Rabano, A., Padovani, A., Squassina, A., de Mendonca, A., Arias Pastor, A., Kok, A.A.L., Meggy, A., Pastor, A.B., Espinosa, A., Corma-Gomez, A., Martin Montes, A., Sanabria, A., DeStefano, A.L., Schneider, A., Haapasalo, A., Kinhult Stahlbom, A., Tybjaerg-Hansen, A., Hartmann, A.M., Spottke, A., Corbaton-Anchuelo, A., Rongve, A., Borroni, B., Arosio, B., Nacmias, B., Nordestgaard, B.G., Kunkle, B.W., Charbonnier, C., Abdelnour, C., Masullo, C., Martinez Rodriguez, C., Munoz-Fernandez, C., Dufouil, C., Graff, C., Ferreira, C.B., Chillotti, C., Reynolds, C.A., Fenoglio, C., Van Broeckhoven, C., Clark, C., Pisanu, C., Satizabal, C.L., Holmes, C., Buiza-Rueda, D., Aarsland, D., Rujescu, D., Alcolea, D., Galimberti, D., Wallon, D., Seripa, D., Grunblatt, E., Dardiotis, E., Duzel, E., Scarpini, E., Conti, E., Rubino, E., Gelpi, E., Rodriguez-Rodriguez, E., Duron, E., Boerwinkle, E., Ferri, E., Tagliavini, F., Kucukali, F., Pasquier, F., Sanchez-Garcia, F., Mangialasche, F., Jessen, F., Nicolas, G., Selbaek, G., Ortega, G., Chene, G., Hadjigeorgiou, G., Rossi, G., Spalletta, G., Giaccone, G., Grande, G., Binetti, G., Papenberg, G., Hampel, H., Bailly, H., Zetterberg, H., Soininen, H., Karlsson, I.K., Alvarez, I., Appollonio, I., Giegling, I., Skoog, I., Saltvedt, I., Rainero, I., Rosas Allende, I., Hort, J., Diehl-Schmid, J., Van Dongen, J., Vidal, J.S., Lehtisalo, J., Wiltfang, J., Thomassen, J.Q., Kornhuber, J., Haines, J.L., Vogelgsang, J., Pineda, J. A., Fortea, J., Popp, J., Deckert, J., Buerger, K., Morgan, K., Fliessbach, K., Sleegers, K., Molina-Porcel, L., Kilander, L., Weinhold, L., Farrer, L.A., Wang, L.S., Kleineidam, L., Farotti, L., Parnetti, L., Tremolizzo, L., Hausner, L., Benussi, L., Froelich, L., Ikram, M.A., Deniz-Naranjo, M.C., Tsolaki, M., Rosende-Roca, M., Lowenmark, M., Hulsman, M., Spallazzi, M., Pericak-Vance, M.A., Esiri, M., Bernal Sanchez-Arjona, M., Dalmasso, M.C., Martinez-Larrad, M.T., Arcaro, M., Nothen, M.M., Fernandez-Fuertes, M., Dichgans, M., Ingelsson, M., Herrmann, M.J., Scherer, M., Vyhnalek, M., Kosmidis, M.H., Yannakoulia, M., Schmid, M., Ewers, M., Heneka, M.T., Wagner, M., Scamosci, M., Kivipelto, M., Hiltunen, M., Zulaica, M., Alegret, M., Fornage, M., Roberto, N., van Schoor, N.M., Seidu, N.M., Banaj, N., Armstrong, N.J., Scarmeas, N., Scherbaum, N., Goldhardt, O., Hanon, O., Peters, O., Skrobot, O.A., Quenez, O., Lerch, O., Bossu, P., Caffarra, P., Dionigi Rossi, P., Sakka, P., Hoffmann, P., Holmans, P.A., Fischer, P., Riederer, P., Yang, Q., Marshall, R., Kalaria, R.N., Mayeux, R., Vandenberghe, R., Cecchetti, R., Ghidoni, R., Frikke-Schmidt, R., Sorbi, S., Hagg, S., Engelborghs, S., Helisalmi, S., Botne Sando, S., Kern, S., Archetti, S., Boschi, S., Fostinelli, S., Gil, S., Mendoza, S., Mead, S., Ciccone, S., Djurovic, S., Heilmann-Heimbach, S., Riedel-Heller, S., Kuulasmaa, T., Del Ser, T., Lebouvier, T., Polak, T., Ngandu, T., Grimmer, T., Bessi, V., Escott-Price, V., Giedraitis, V., Deramecourt, V., Maier, W., Jian, X., Pijnenburg, Y.A.L., contributors, E., group, G.A.s., consortium, D., Igap, consortia, P.-A., Kehoe, P.G., Garcia-Ribas, G., Sanchez-Juan, P., Pastor, P., Perez-Tur, J., Pinol-Ripoll, G., Lopez de Munain, A., Garcia-Alberca, J.M., Bullido, M. J., Alvarez, V., Lleo, A., Real, L.M., Mir, P., Medina, M., Scheltens, P., Holstege, H., Marquie, M., Saez, M.E., Carracedo, A., Amouyel, P., Schellenberg, G.D., Williams, J., Seshadri, S., van Duijn, C.M., Mather, K.A., Sanchez-Valle, R., Serrano-Rios, M., Orellana, A., Tarraga, L., Blennow, K., Huisman, M., Andreassen, O.A., Posthuma, D., Clarimon, J., Boada, M., van der Flier, W.M., Ramirez, A., Lambert, J.C., van der Lee, S.J., Ruiz, A., 2021. Common variants in Alzheimer's disease and risk stratification by polygenic risk scores. Nat Commun 12, 3417.

Del Puppo, M., Kienle, M.G., Petroni, M.L., Crosignani, A., Podda, M., 1998. Serum 27-hydroxycholesterol in patients with primary biliary cirrhosis suggests alteration of cholesterol catabolism to bile acids via the acidic pathway. J. Lipid Res. 39, 2477–2482.

Dietschy, J.M., Turley, S.D., 2001. Cholesterol metabolism in the brain. Curr. Opin. Lipidol. 12, 105–112.

Edwards, F.A., 2019. A Unifying Hypothesis for Alzheimer's Disease: From Plaques to Neurodegeneration. Trends Neurosci. 42, 310–322.

Feringa, F.M., van der Kant, R., 2021. Cholesterol and Alzheimer's Disease; From Risk Genes to Pathological Effects. Front. Aging Neurosci. 13, 690372.

Ferri, N., 2012. Proprotein convertase subtilisin/kexin type 9: from the discovery to the development of new therapies for cardiovascular diseases. Scientifica (cairo) 2012, 927352.

Forner, S., Kawauchi, S., Balderrama-Gutierrez, G., Kramar, E.A., Matheos, D.P., Phan, J., Javonillo, D.I., Tran, K.M., Hingco, E., da Cunha, C., Rezaie, N., Alcantara, J.A., Baglietto-Vargas, D., Jansen, C., Neumann, J., Wood, M.A., MacGregor, G.R., Mortazavi, A., Tenner, A.J., LaFerla, F.M., Green, K.N., 2021. Systematic phenotyping and characterization of the 5xFAD mouse model of Alzheimer's disease. Sci. Data 8, 270.

Giovannoni, F., Quintana, F.J., 2020. The Role of Astrocytes in CNS Inflammation. Trends Immunol. 41, 805–819.

Hollingworth, P., Harold, D., Sims, R., Gerrish, A., Lambert, J.C., Carrasquillo, M.M., Abraham, R., Hamshere, M.L., Pahwa, J.S., Moskvina, V., Dowzell, K., Jones, N., Stretton, A., Thomas, C., Richards, A., Ivanov, D., Widdowson, C., Chapman, J., Lovestone, S., Powell, J., Proitsi, P., Lupton, M.K., Brayne, C., Rubinsztein, D.C., Gill, M., Lawlor, B., Lynch, A., Brown, K.S., Passmore, P.A., Craig, D., McGuinness, B., Todd, S., Holmes, C., Mann, D., Smith, A.D., Beaumont, H., Warden, D., Wilcock, G., Love, S., Kehoe, P.G., Hooper, N.M., Vardy, E.R., Hardy, J., Mead, S., Fox, N.C., Rossor, M., Collinge, J., Maier, W., Jessen, F., Ruther, E., Schurmann, B., Heun, R., Kolsch, H., van den Bussche, H., Heuser, I., Kornhuber, J., Wiltfang, J., Dichgans, M., Frolich, L., Hampel, H., Gallacher, J., Hull, M., Rujescu, D., Giegling, I., Goate, A.M., Kauwe, J.S., Cruchaga, C., Nowotny, P., Morris, J.C., Mayo, K., Sleegers, K., Bettens, K., Engelborghs, S., De Deyn, P.P., Van Broeckhoven, C., Livingston, G., Bass, N.J., Gurling, H., McQuillin, A., Gwilliam, R., Deloukas, P., Al-Chalabi, A., Shaw, C.E., Tsolaki, M., Singleton, A.B., Guerreiro, R., Muhleisen, T.W., Nothen, M.M., Moebus, S., Jockel, K.H., Klopp, N., Wichmann, H.E., Pankratz, V.S., Sando, S.B., Aasly, J.O., Barcikowska, M., Wszolek, Z.K., Dickson, D.W., Graff-Radford, N.R., Petersen, R.C., Alzheimer's Disease Neuroimaging, I., van Duijn, C.M., Breteler, M.M., Ikram, M.A., DeStefano, A.L., Fitzpatrick, A.L., Lopez, O., Launer, L.J., Seshadri, S., consortium, C., Berr, C., Campion, D., Epelbaum, J., Dartigues, J.F., Tzourio, C., Alperovitch, A., Lathrop, M., consortium, E., Feulner, T.M., Friedrich, P., Riehle, C., Krawczak, M., Schreiber, S., Mayhaus, M., Nicolhaus, S., Wagenpfeil, S., Steinberg, S., Stefansson, H., Stefansson, K., Snaedal, J., Bjornsson, S., Jonsson, P.V., Chouraki, V., Genier-Boley, B., Hiltunen, M., Soininen, H., Combarros, O., Zelenika, D., Delepine, M., Bullido, M.J., Pasquier, F., Mateo, I., Frank-Garcia, A., Porcellini, E., Hanon, O., Coto, E., Alvarez, V., Bosco, P., Siciliano, G., Mancuso, M., Panza, F., Solfrizzi, V., Nacmias, B., Sorbi, S., Bossu, P., Piccardi, P., Arosio, B., Annoni, G., Seripa, D., Pilotto, A., Scarpini, E., Galimberti, D., Brice, A., Hannequin, D., Licastro, F., Jones, L., Holmans, P.A., Jonsson, T., Riemenschneider, M., Morgan, K., Younkin, S.G., Owen, M.J., O'Donovan, M., Amouyel, P., Williams, J., 2011. Common variants at ABCA7, MS4A6A/MS4A4E, EPHA1, CD33 and CD2AP are associated with Alzheimer's disease. Nat Genet 43, 429-435.

Jack Jr., C.R., Knopman, D.S., Jagust, W.J., Petersen, R.C., Weiner, M.W., Aisen, P.S., Shaw, L.M., Vemuri, P., Wiste, H.J., Weigand, S.D., Lesnick, T.G., Pankratz, V.S., Donohue, M.C., Trojanowski, J.Q., 2013. Tracking pathophysiological processes in Alzheimer's disease: an updated hypothetical model of dynamic biomarkers. Lancet Neurol. 12, 207–216.

Jaen, R.I., Povo-Retana, A., Rosales-Mendoza, C., Capillas-Herrero, P., Sanchez-Garcia, S., Martin-Sanz, P., Mojena, M., Prieto, P., Bosca, L., 2022. Functional Crosstalk between PCSK9 Internalization and Pro-Inflammatory Activation in Human Macrophages: Role of Reactive Oxygen Species Release. Int. J. Mol. Sci. 23.

Jones, L., Holmans, P.A., Hamshere, M.L., Harold, D., Moskvina, V., Ivanov, D., Pocklington, A., Abraham, R., Hollingworth, P., Sims, R., Gerrish, A., Pahwa, J.S., Jones, N., Stretton, A., Morgan, A.R., Lovestone, S., Powell, J., Proitsi, P., Lupton, M. K., Brayne, C., Rubinsztein, D.C., Gill, M., Lawlor, B., Lynch, A., Morgan, K., Brown, K.S., Passmore, P.A., Craig, D., McGuinness, B., Todd, S., Holmes, C., Mann, D., Smith, A.D., Love, S., Kehoe, P.G., Mead, S., Fox, N., Rossor, M., Collinge, J., Maier, W., Jessen, F., Schurmann, B., Heun, R., Kolsch, H., van den Bussche, H., Heuser, I., Peters, O., Kornhuber, J., Wiltfang, J., Dichgans, M., Frolich, L., Hampel, H., Hull, M., Rujescu, D., Goate, A.M., Kauwe, J.S., Cruchaga, C., Nowotny, P., Morris, J.C., Mayo, K., Livingston, G., Bass, N.J., Gurling, H., McQuillin, A., Gwilliam, R., Deloukas, P., Al-Chalabi, A., Shaw, C.E., Singleton, A.B., Guerreiro, R., Muhleisen, T.W., Nothen, M.M., Moebus, S., Jockel, K.H., Klopp, N., Wichmann, H.E., Ruther, E., Carrasquillo, M.M., Pankratz, V.S., Younkin, S.G., Hardy, J., O'Donovan, M.C., Owen, M.J., Williams, J., 2010. Genetic evidence implicates the immune system and cholesterol metabolism in the aetiology of Alzheimer's disease. PLoS One 5, e13950.

Kinney, J.W., Bemiller, S.M., Murtishaw, A.S., Leisgang, A.M., Salazar, A.M., Lamb, B.T., 2018. Inflammation as a central mechanism in Alzheimer's disease. Alzheimers Dement (n y) 4, 575–590.

Koronyo, Y., Salumbides, B.C., Sheyn, J., Pelissier, L., Li, S., Ljubimov, V., Moyseyev, M., Daley, D., Fuchs, D.T., Pham, M., Black, K.L., Rentsendorj, A., Koronyo-Hamaoui, M., 2015. Therapeutic effects of glatiramer acetate and grafted CD115(+) monocytes in a mouse model of Alzheimer's disease. Brain 138, 2399–2422.

Koronyo-Hamaoui, M., Sheyn, J., Hayden, E.Y., Li, S., Fuchs, D.T., Regis, G.C., Lopes, D. H.J., Black, K.L., Bernstein, K.E., Teplow, D.B., Fuchs, S., Koronyo, Y., Rentsendorj, A., 2020. Peripherally derived angiotensin converting enzyme-enhanced macrophages alleviate Alzheimer-related disease. Brain 143, 336–358.

Koutsodendris, N., Nelson, M.R., Rao, A., Huang, Y., 2022. Apolipoprotein E and Alzheimer's Disease: Findings, Hypotheses, and Potential Mechanisms. Annu. Rev. Pathol. 17, 73–99.

Kysenius, K., Muggalla, P., Matlik, K., Arumae, U., Huttunen, H.J., 2012. PCSK9 regulates neuronal apoptosis by adjusting ApoER2 levels and signaling. Cell. Mol. Life Sci. 69, 1903–1916.

Lau, J.K.Y., Tian, M., Shen, Y., Lau, S.F., Fu, W.Y., Fu, A.K.Y., Ip, N.Y., 2021. Melanocortin receptor activation alleviates amyloid pathology and glial reactivity in an Alzheimer's disease transgenic mouse model. Sci. Rep. 11, 4359.

Li, D., Zhang, J., Liu, Q., 2022. Brain cell type-specific cholesterol metabolism and implications for learning and memory. Trends Neurosci. 45, 401–414.

Liu, L.S., Bai, X.Q., Gao, Y., Wu, Q., Ren, Z., Li, Q., Pan, L.H., He, N.Y., Peng, J., Tang, Z. H., 2017. PCSK9 Promotes oxLDL-Induced PC12 Cell Apoptosis Through the Bcl-2/Bax-Caspase 9/3 Signaling Pathway. J. Alzheimers Dis. 57, 723–734.

Liu, A., Frostegard, J., 2018. PCSK9 plays a novel immunological role in oxidized LDL-induced dendritic cell maturation and activation of T cells from human blood and atherosclerotic plaque. J. Intern. Med.

Liu, C.C., Liu, C.C., Kanekiyo, T., Xu, H., Bu, G., 2013. Apolipoprotein E and Alzheimer disease: risk, mechanisms and therapy. Nat. Rev. Neurol. 9, 106–118.

Liu, M., Wu, G., Baysarowich, J., Kavana, M., Addona, G.H., Bierilo, K.K., Mudgett, J.S., Pavlovic, G., Sitlani, A., Renger, J.J., Hubbard, B.K., Fisher, T.S., Zerbinatti, C.V., 2010. PCSK9 is not involved in the degradation of LDL receptors and BACE1 in the adult mouse brain. J. Lipid Res. 51, 2611–2618.

Lucin, K.M., O'Brien, C.E., Bieri, G., Czirr, E., Mosher, K.I., Abbey, R.J., Mastroeni, D.F., Rogers, J., Spencer, B., Masliah, E., Wyss-Coray, T., 2013. Microglial beclin 1 regulates retromer trafficking and phagocytosis and is impaired in Alzheimer's disease. Neuron 79, 873–886.

Mahley, R.W., 2016. Central Nervous System Lipoproteins: ApoE and Regulation of Cholesterol Metabolism. Arterioscler. Thromb. Vasc. Biol. 36, 1305–1315.

Man, S.M., Kanneganti, T.D., 2015. Regulation of inflammasome activation. Immunol. Rev. 265, 6–21.

Mazura, A.D., Ohler, A., Storck, S.E., Kurtyka, M., Scharfenberg, F., Weggen, S., Becker-Pauly, C., Pietrzik, C.U., 2022. PCSK9 acts as a key regulator of Abeta clearance across the blood-brain barrier. Cell. Mol. Life Sci. 79, 212.

McFarlane, O., Kedziora-Kornatowska, K., 2020. Cholesterol and Dementia: A Long and Complicated Relationship. Curr. Aging Sci. 13, 42–51.

Oblak, A.L., Lin, P.B., Kotredes, K.P., Pandey, R.S., Garceau, D., Williams, H.M., Uyar, A., O'Rourke, R., O'Rourke, S., Ingraham, C., Bednarczyk, D., Belanger, M., Cope, Z.A., Little, G.J., Williams, S.G., Ash, C., Bleckert, A., Ragan, T., Logsdon, B.A., Mangravite, L.M., Sukoff Rizzo, S.J., Territo, P.R., Carter, G.W., Howell, G.R., Sasner, M., Lamb, B.T., 2021. Comprehensive Evaluation of the 5XFAD Mouse Model for Preclinical Testing Applications: A MODEL-AD Study. Front. Aging Neurosci. 13, 713726.

Ohno, M., Cole, S.L., Yasvoina, M., Zhao, J., Citron, M., Berry, R., Disterhoft, J.F., Vassar, R., 2007. BACE1 gene deletion prevents neuron loss and memory deficits in 5XFAD APP/PS1 transgenic mice. Neurobiol. Dis. 26, 134–145.

Papotti, B., Adorni, M.P., Marchi, C., Zimetti, F., Ronda, N., Panighel, G., Lupo, M.G., Vilella, A., Giuliani, D., Ferri, N., Bernini, F., 2022. PCSK9 Affects Astrocyte Cholesterol Metabolism and Reduces Neuron Cholesterol Supplying In Vitro: Potential Implications in Alzheimer's Disease. Int J Mol Sci 23.

Paquette, M., Saavedra, Y.G.L., Poirier, J., Theroux, L., Dea, D., Baass, A., Dufour, R., 2018. Loss-of-Function PCSK9 Mutations Are Not Associated With Alzheimer Disease. J. Geriatr. Psychiatry Neurol. 31, 90–96.

Paxinos, G., Franklin, K.B.J., 2019. Paxinos and Franklin's the Mouse Brain in Stereotaxic Coordinates.

Picard, C., Poirier, A., Belanger, S., Labonte, A., Auld, D., Poirier, J., Group, P.-A.R., 2019. Proprotein convertase subtilisin/kexin type 9 (PCSK9) in Alzheimer's disease: A genetic and proteomic multi-cohort study. PLoS One 14, e0220254.

Poirier, S., Mayer, G., Benjannet, S., Bergeron, E., Marcinkiewicz, J., Nassoury, N., Mayer, H., Nimpf, J., Prat, A., Seidah, N.G., 2008. The proprotein convertase PCSK9 induces the degradation of low density lipoprotein receptor (LDLR) and its closest family members VLDLR and ApoER2. J. Biol. Chem. 283, 2363–2372.

Ricci, C., Ruscica, M., Camera, M., Rossetti, L., Macchi, C., Colciago, A., Zanotti, I., Lupo, M.G., Adorni, M.P., Cicero, A.F.G., Fogacci, F., Corsini, A., Ferri, N., 2018. PCSK9 induces a pro-inflammatory response in macrophages. Sci. Rep. 8, 2267.

Rigillo, G., Vilella, A., Benatti, C., Schaeffer, L., Brunello, N., Blom, J.M.C., Zoli, M., Tascedda, F., 2018. LPS-induced histone H3 phospho(Ser10)-acetylation(Lys14) regulates neuronal and microglial neuroinflammatory response. Brain Behav. Immun. 74, 277–290.

Runfola, M., Perni, M., Yang, X., Marchese, M., Bacci, A., Mero, S., Santorelli, F.M., Polini, B., Chiellini, G., Giuliani, D., Vilella, A., Bodria, M., Daini, E., Vandini, E., Rudge, S., Gul, S., Wakelam, M.O.J., Vendruscolo, M., Rapposelli, S., 2021. Identification of a Thyroid Hormone Derivative as a Pleiotropic Agent for the Treatment of Alzheimer's Disease. Pharmaceuticals (Basel) 14.

Sadleir, K.R., Kandalepas, P.C., Buggia-Prevot, V., Nicholson, D.A., Thinakaran, G., Vassar, R., 2016. Presynaptic dystrophic neurites surrounding amyloid plaques are sites of microtubule disruption, BACE1 elevation, and increased Abeta generation in Alzheimer's disease. Acta Neuropathol. 132, 235–256.

Seidah, N.G., Benjannet, S., Wickham, L., Marcinkiewicz, J., Jasmin, S.B., Stifani, S., Basak, A., Prat, A., Chretien, M., 2003. The secretory proprotein convertase neural apoptosis-regulated convertase 1 (NARC-1): liver regeneration and neuronal differentiation. PNAS 100, 928–933.

Tang, Z.H., Peng, J., Ren, Z., Yang, J., Li, T.T., Li, T.H., Wang, Z., Wei, D.H., Liu, L.S., Zheng, X.L., Jiang, Z.S., 2017. New role of PCSK9 in atherosclerotic inflammation promotion involving the TLR4/NF-kappaB pathway. Atherosclerosis 262, 113–122.

Therriault, J., Zimmer, E.R., Benedet, A.L., Pascoal, T.A., Gauthier, S., Rosa-Neto, P., 2022. Staging of Alzheimer's disease: past, present, and future perspectives. Trends Mol. Med.

Villacampa, N., Almolda, B., Vilella, A., Campbell, I.L., Gonzalez, B., Castellano, B., 2015. Astrocyte-targeted production of IL-10 induces changes in microglial reactivity and reduces motor neuron death after facial nerve axotomy. Glia 63, 1166–1184.

Vorhees, C.V., Williams, M.T., 2006. Morris water maze: procedures for assessing spatial and related forms of learning and memory. Nat. Protoc. 1, 848–858.

Wu, M., Zhang, M., Yin, X., Chen, K., Hu, Z., Zhou, Q., Cao, X., Chen, Z., Liu, D., 2021. The role of pathological tau in synaptic dysfunction in Alzheimer's diseases. Transl Neurodegener 10, 45.

Yin, F., 2022. Lipid metabolism and Alzheimer's disease: clinical evidence, mechanistic link and therapeutic promise. FEBS J.

Zimetti, F., Caffarra, P., Ronda, N., Favari, E., Adorni, M.P., Zanotti, I., Bernini, F., Barocco, F., Spallazzi, M., Galimberti, D., Ricci, C., Ruscica, M., Corsini, A., Ferri, N., 2017. Increased PCSK9 Cerebrospinal Fluid Concentrations in Alzheimer's Disease. J. Alzheimers Dis. 55, 315–320.

Zoli, M., Benfenati, F., Pich, E.M., Toffano, G., Fuxe, K., Agnati, L.F., 1990a. Aspects of neural plasticity in the central nervous system-IV. Chemical anatomical studies on the aging brain. Neurochem. Int. 16, 437–449.

Zoli, M., Zini, I., Agnati, L.F., Guidolin, D., Ferraguti, F., Fuxe, K., 1990b. Aspects of neural plasticity in the central nervous system-I. Computer-Assisted Image Analysis Methods. Neurochem Int 16, 383–418.

Zoli, M., Guidolin, D., Agnati, L.F., 1992. Morphometric evaluation of populations of neuronal profiles (cell bodies, dendrites, and nerve terminals) in the central nervous system. Microsc. Res. Tech. 21, 315–337.